Modelling Sea-Level Fingerprints of Glaciated Regions with Low Mantle Viscosity

by

Alan Bartholet

Submitted to the Department of Earth and Environmental Science
in partial fulfillment of the requirements for the degree

Master of Science

at the

UNIVERSITY OF OTTAWA

April 2020

Modelling Sea-Level Fingerprints of Glaciated Regions with Low Mantle Viscosity

by

Alan Bartholet

Submitted to the Department of Earth and Environmental Science
on April 19, 2020, in partial fulfillment of the
requirements for the degree
Master of Science

Abstract

Sea-level fingerprints, the spatial patterns of sea level change resulting from rapid melting of glaciers and ice sheets, play an important role in understanding past and projecting future changes in relative sea level (RSL). Over century timescales, the viscous flow of Earth's interior is a small component of the total deformation due to ice loading in most regions, so fingerprints computed using elastic Earth models are accurate. However, in regions where the viscosity is orders of magnitude lower than the global average, the viscous component of deformation can be significant, in which case it is important to consider models of viscoelastic deformation.

There is evidence that the glaciated regions of Alaska, Western Canada and USA, and the Southern Andes are situated on top of mantle regions in which the local viscosity is several orders of magnitude lower than typical global mean values. The goal of this work is to determine the importance of viscous flow in computing RSL fingerprints associated with future ice mass loss from these regions. Version 5.0 of the Randolph Glacier Inventory is used to estimate the ice load distribution required for calculating sea-level fingerprints. For the glaciated regions that have lower than average viscosity, fingerprints were calculated using an elastic Earth model and a 3D viscoelastic model to quantify the influence of viscous flow on the predicted sea level changes. Using glacier mass loss values for the intermediate future climate scenario Representative Concentration Pathway (RCP) 4.5, the global sea level response was computed at 2100 CE relative to 2010 CE due to melting from all glacier regions. On comparing the results of the two models it was found that ice-load-induced viscous flow contributes significantly (more than a few cm) to the RSL fingerprints only in near-field regions. However, in these regions, the non-elastic contribution can be 10s of cm. For example, at Juneau, USA the elastic calculation gave relative sea level changes of $\sim -45\,\mathrm{cm}$, compared to $\sim -120\,\mathrm{cm}$ based on the viscoelastic calculation.

Acknowledgments

I would first like to express my deepest appreciation to my supervisor, Glenn Milne, thank you for your patience, guidance, and expertise throughout my studies. I would also like to thank the other members my research group in Ottawa who shared their knowledge with me in understanding many new concepts.

Additionally I want to express my gratitude to Ryan Love for his help on modeling the ice loads and especially to Konstantin Latychev, who spent so much time providing advice and support on working with the 3-D Earth model.

A very special thanks goes to my loving wife, Samaneh Bartholet, who provided the initial encouragement to pursue doing this research and who has supported me in so many ways over the years, I am forever grateful.

Lastly, thank the Natural Sciences and Engineering Research Council (NSERC) of Canada for providing the funding for me to do this research and expand my understanding of the wonderfully complex world around us.

Contents

List of Figures

1

Introduction

1.1 Motivation

For the past two millennia, up until the 20th century, there has been relatively little change in global mean sea level (GMSL) (Masson-Delmotte et al., 2013). This period of relative sea level stability made coastal regions attractive for human settlement: alluvial plains and deltas next to coastlines presented fertile land for agricultural production, mild climate made life more comfortable and easier, and coastal waters provided access to the oceans for both resources and transportation. Over time these settlements would become hubs for trade and commerce (Griggs, 2017).

Settlements in coastal lowlands are particularly vulnerable to climate change due to sea-level rise, stronger and more frequent storms, and other seaward hazards. Despite this, these densely populated areas continue to grow. During the 20th century

and into the 21st, major coastal cities continued to expand, with eight of the world's largest cities on the coast having a cumulative population of just over 200 million. Of the twenty-five largest cities in the world, eighteen are coastal and have a combined population of 357 million people, almost 5% of the world's population (Griggs, 2017).

Predicting sea-level rise is one of the great scientific problems of our time. The estimation of GMSL rise is a non-trivial task and estimating local and regional sea level change is even more challenging where the vertical movement of either the ocean or land surface along any coast can cause (relative) sea-level change (see Section 1.2). A variety of processes may drive changes in the height of the ocean floor and ocean surface and the combination of these processes produces a complex pattern of sea level change that varies through time as the relative contribution of each process often changes. While the global average change provides a useful single value which reflects the contribution of multiple processes and does represent a good estimate of sea level change at many coastal locations, various regional processes that produce a strong signal can result in large departures from the global average value (Church et al., 2013). As a result, predicting sea level at the regional scale requires an in-depth understanding of numerous physical processes that have a range of spacial scales and response times (see Section 1.2.1).

This thesis will focus on the contribution of glaciers and ice caps (GIC) to future sea-level rise, and includes glaciers on the periphery of Greenland and Antartica but not the ice sheets themselves. Even though GIC represent less than one percent of the land ice on Earth, their melting has contributed nearly a third of the observed sea level rise since 1971 and is projected to be the second large contributor to sea level rise over the next century (Church et al., 2013). As a result, understanding how these melting GIC affect global to local sea levels is vital in mitigating the impact rising sea level will have on coastal communities.

Over the 20th century, the GMSL rise has been approximately $1.3\,\mathrm{mm\,a^{-1}}$ with this rate doubling over the past two decades (Masson-Delmotte et al., 2013). Compared to observations of wave and tidal oscillations, which can be orders of magnitude larger, these rates may seem to be small. However, when they persist over long time

intervals, the magnitude bears important ramifications for low-lying, heavily populated coastal regions, where small increases in sea level can inundate large land areas. Also, as mean sea level rises, the return period for sea levels of a given height decreases, leading to more frequent flooding events. Currently, over 130 port cities are now under threat of rising sea level (Nicholls et al., 2008; Griggs, 2017). The research presented in this thesis is a contribution towards improving our understanding of future sea-level change associated with melting GIC. This work is motivated by the need to produce improved regional sea-level projections to better inform the relevant stakeholders.

1.2 Sea-level change

While it is commonly thought that "sea level" is where the ocean meets the land, it is actually more complicated than that. For scientific purposes, sea level is defined in two different ways. Relative sea level (RSL) is defined as the height of the sea surface relative to the land surface (strictly speaking the ocean floor (Figure 1-1)), both of which may be changing height relative to the center of the Earth.

Geocentric, or absolute, sea level (Figure 1-1) is defined as sea-surface height relative to the reference ellipsoid. The reference ellipsoid is a theoretical surface of ellipsoidal geometry that best fits the mean level of the ocean surface, or geoid, and is centred at the center of mass of the Earth. Geocentric sea level is measured using satellite altimetry and while it provides a robust measurement of shifts in the sea surface as a result of climate change, RSL is more relevant in the context of coastal evolution and to assess local impacts of sea level change (Milne, 2014).

RSL change is, therefore, often a combination of processes operating within the solid earth, oceans, and atmosphere, with timescales ranging from hours to millions of years and spacial scales of less than 1 km to global. Solid earth processes that affect RSL include tectonics, sediment compaction, and isostatic adjustment as they can all result in vertical motion of the solid Earth. Climate processes (i.e. those operating in the atmosphere, oceans, and cryosphere) that influence sea level include changes

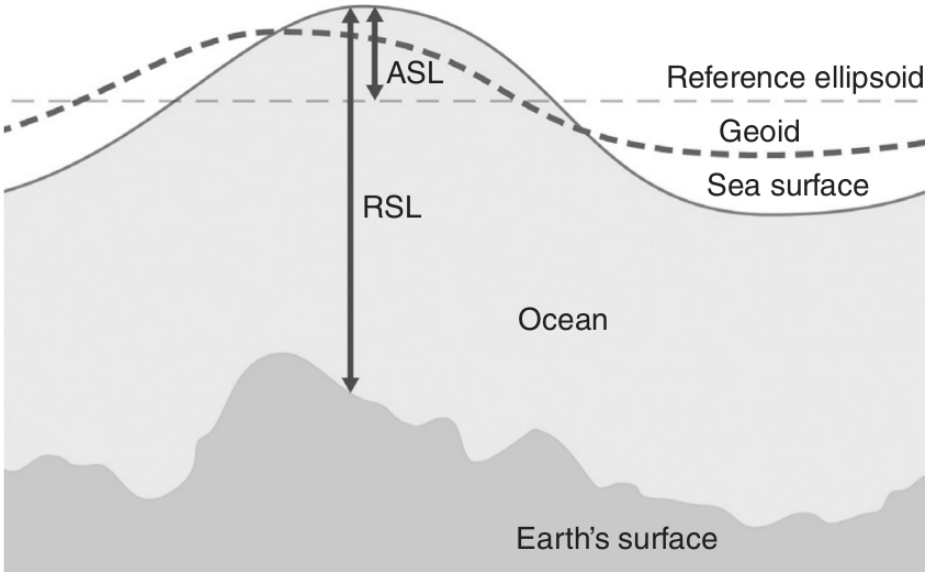

Figure 1-1. Relative sea level (RSL) is the height difference between the Earth's solid surface and the sea surface. At coastlines where the two surfaces meet, RSL is zero. The geoid is an equipotential surface of the Earth's gravity field and is the approximate mean position of the ocean surface over time periods greater than a few decades. The reference ellipsoid is the best-fitting geometric surface to the geoid. Absolute sea level (ASL), or geocentric sea level, is the height of the ocean surface with respect to the reference ellipsoid (Milne, 2014).

in ocean temperature resulting in the expansion and contraction of ocean water, variations in the volume of glaciers and ice sheets, and changes in ocean currents.

Over the last twenty thousand years, the Earth's climate has warmed significantly, with an increase of 4–5 °C in global mean surface temperature causing the melting of massive quantities of land ice around the globe. As a result, GMSL rose by ∼130 m and stabilized ∼6000 years ago to within a few meters of present day sea level. Tide gauge records for the period 1901-2010 indicate that GMSL rose at an average rate of $\sim 1.7\,\mathrm{mm\,a^{-1}}$ for a total sea level rise of ∼19 cm (Church et al., 2013). Satellite altimetry records for the period of 1993–2012 give a rate of GMSL rise of $\sim 3.2\,\mathrm{mm\,a^{-1}}$ (Church et al., 2013).

Changes in both solid Earth and climate factors can produce significant deviations in local and regional sea level changes when compared to estimates of the GMSL change. For example, in the Gulf of Bothnia, along the northern Swedish coast, local sea level is falling at a rate of $\sim 10\,\mathrm{mm\,a^{-1}}$ due to continuing uplift resulting from

melting of continental ice after the last glacial period. Conversely, local sea level south of Bangkok rose at a rate of $\sim$20 mm a^{-1} from 1960-2005 due mostly to land subsidence from ground water extraction (Masson-Delmotte et al., 2013).

In this section I introduce processes that will contribute to future sea-level change on global and regional scales. One of these processes is glacial isostatic adjustment (GIA) which explains how the influence of past changes in land ice contribute to future sea levels due to the ongoing viscous deformation of the solid Earth. Additionally, contemporary and future changes in land ice will also drive vertical land motion which in turn will result in relative sea level change; this process is the focus of Chapter Chapter 2, which represents the original research contribution of this thesis. The other process I will introduce is the influence of changes in ocean density, known as the steric component of sea-level change.

1.2.1 Key processes that will contribute to future sea-level change

The warming of Earth's climate will influence sea-level change through mainly two processes: melting of land ice and changes in ocean properties (temperature and salinity). In this section I provide a qualitative overview of the relevant physics associated with these processes.

1.2.1.1 Changes in land ice extent

Past changes

There have been at least five major ice ages in Earth's past. Within these ice ages the Earth experiences glacial periods marked by colder temperatures and glacial advancement and interglacial periods marked by warmer temperatures and glacial retreat. The most recent glacial period occurred from 100,000–11,700 years ago when massive ice sheets covered parts of Europe, Siberia, and North America. During this time the ice sheets would extend and retreat periodically, with the maximum extent, known as the last glacial maximum, occurring $\sim$20,000 years ago.

During the past ∼700,000 years, Earth's climate has undergone an alternating cycle of glacial and interglacial periods with a dominant periodicity of 100,000 years. These cycles resulted in large-scale changes in the spatial distribution of land ice. During a glacial period, lower temperatures cause ice sheets to grow at higher latitudes, and as a result the total volume of water in the oceans decrease. Conversely, during an interglacial period, warmer temperatures cause the ice sheets to retreat, thus returning the water that was previously locked up in continental ice to the ocean (Ruddiman, 2001). This movement of water and ice over the surface of the Earth during glacial cycles results in mass loading on the lithosphere. In response to this loading the Earth deforms, subsiding under the load of ice sheets and uplifting when the ice sheets melt.

The deformation that takes place during this loading and unloading of mass is isostatic. The principle of isostasy describes how the solid Earth attempts to return to a state of isostatic equilibrium following a change in the surface load distribution. In the Pratt theory of isostasy, the Earth's lithosphere effectively floats on the asthenosphere, and the elevation at which it sits depends on the total mass above this depth of floatation (or compensation). As mass is added or removed from the surface, the change in mass above the compensation depth is accommodated by a vertical deflection at the lithosphere-asthenosphere boundary that results in a change in the buoyancy force. The rate of this deflection is governed by the viscosity of rock in this region. In reality, the compensation (buoyancy) forces are produced at any depth where there is a density contrast, assuming the change in surface load is of large enough spatial scale to result in deformation to a given depth.

GIA can be described as the isostatic deformation resulting from ice and water loading on the Earth's surface during glacial cycles. A sufficiently large mass of ice will cause the surface of the Earth to flex, resulting in the depression of the Earth under the ice load and uplift of a bulge around the periphery of the ice as mantle material displaced under the ice flows outwards towards the periphery. During deglaciation, as the ice mass is reduced, the previously glaciated area will uplift and the peripheral bulge will subside (Figure 1-2). The rate and amplitude of this defor-

mation is governed by the rheology of solid earth material. To a good approximation, the Earth response is viscoelastic such that there is a relatively small instantaneous uplift of the Earth's surface which is governed by the elastic properties of the solid Earth. The more significant viscous response is delayed due the highly viscous nature of the mantle material below the lithosphere. As a result, it takes tens of thousands of years for the Earth to return to a state of equilibrium after an ice mass has stopped melting (or has completely melted).

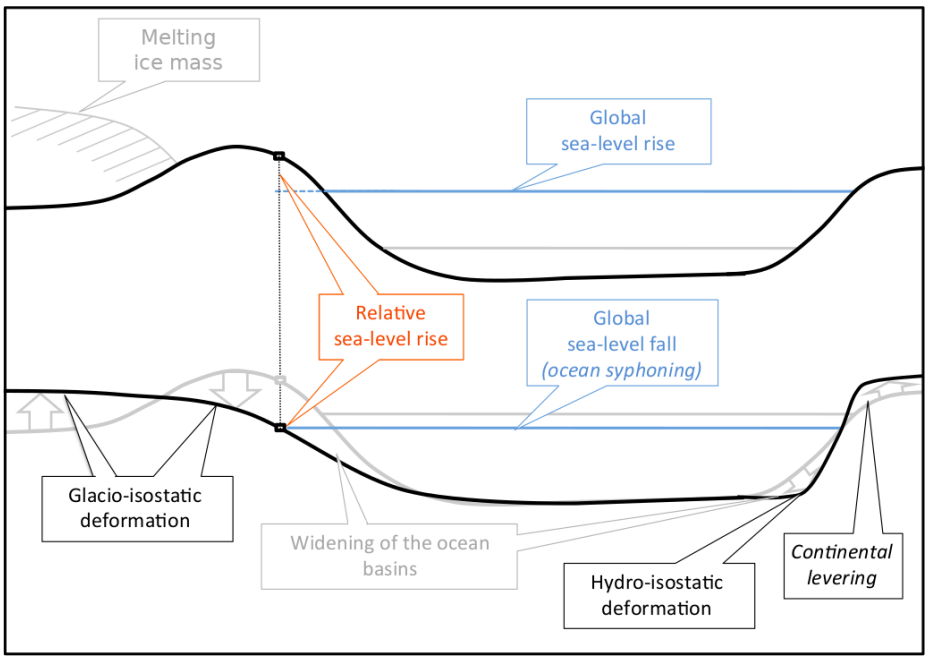

Figure 1-2. Top: Due to the high viscosity of the mantle the solid Earth remains deformed even after the ice mass has melted and GMSL has risen. For clarity, the gravitational effects are not depicted (see Figure 1-5). Bottom: Over time the crust near the former ice sheet progressively relaxes due to glacio-isostatic deformation, while the ocean basin widens and deepens due to hydro-isostatic deformation (Botella, 2015).

Hydro-isostatic deformation is another consequence of glaciation and deglaciation, the massive influx of melt water during deglaciation results in additional pressure on the seafloor and causes it to subside in many areas of the ocean. This is most noticeable along ocean-continent margins at low latitudes (away from major ice sheets) where the increased ocean load results in subsidence of the sea floor surrounding continents and an uplifting of the continents due to flexing of the lithosphere and the

flow of mantle material from oceanic to continental mantle. This process is referred to as "continental levering" (Clark et al., 1978). In addition to local changes in RSL, hydro-isostasy also influences global sea level by changing the volume of the ocean basins.

The GIA signal from past glacial loading events is a significant contributor to both contemporary vertical land motion and relative sea-level change and should be considered when making relative sea-level projections (Love et al., 2016; Yousefi et al., 2018).

Future changes

Around the world, glaciers and ice sheets are losing mass and retreating. For example, observations since 1850 show that, on a global scale, the rate of glacier mass loss in the early 21st-century is without precedent for the observation period (and potentially for all recoded history) (Zemp et al., 2015). The same physical processes that caused sea-level changes in the past due to ice mass changes (glacial cycles) will also affect future sea-level changes. However, because these changes are associated with contemporary and future ice mass change they are not termed GIA, but rather "sea-level fingerprints". In this section I will briefly describe the processes through which glaciers and ice sheets change mass and contribute to sea level change.

Glaciation occurs when topographical features and climate conditions allow for the multi-year accumulation of snow. As this snow persists over several years it slowly compresses into firn (mean density of $600\,\mathrm{kg\,m^{-3}}$) and eventually into ice (mean density of $\sim 900\,\mathrm{kg\,m^{-3}}$) (Cuffey and Paterson, 2010). Gravitational forces cause the ice to flow towards lower, warmer, elevations where the loss of snow and ice, referred to as ablation, is greater than the accumulation. The mass balance of a glacier or ice sheet is calculated as the sum of all ablation and accumulation processes (Figure 1-3). When the mass balance is positive, the glacier grows and when it is negative the glacier recedes. In most regions, snow fall is the dominant form of accumulation, however, the refreezing of liquid water at high altitudes or in polar regions is another source of accumulation. Runoff from surface melt is the predominant form of ablation

in most regions, but calving (when a mass of ice breaks away from the glacier into a body of water producing an iceberg) or sublimation can also dominate in some regions. Wind and avalanches cause a redistribution of snow and may result in both ablation and/or accumulation.

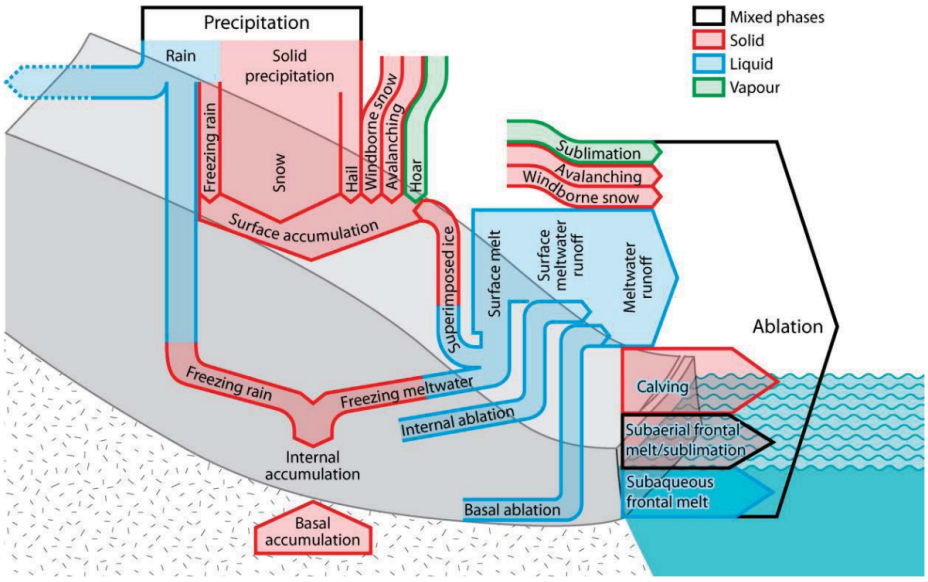

Figure 1-3. Glacier mass balance components. The size of the arrows are cosmetic and do not express mass transfer physical pathways (Cogley et al., 2011).

Heat energy received by or lost from a glacier, in part, determines the mass balance and temperature variation of the glacier and takes place predominantly at the upper surface. The heat energy coming into a glacier includes short-wave solar radiation, long-wave radiation from water vapour or clouds, turbulent transfer from warm air, the heat released from the freezing of liquid water or the condensation of hoarfrost or dew, and the upward conduction from warmer lower layers. The heat energy leaving a glacier consists of the outgoing long-wave radiation, turbulent transfer of colder air, the energy required for the evaporation, sublimation, or melting of ice, and downward conduction to lower layers.

While the two ice sheets currently found on Earth are located in the high latitudes, GIC are mostly located in the mid- and low-latitudes. At these latitudes, the greatest source of heat is the incoming solar radiation and the majority of the heat lost by the glaciers is expended in melting the ice. However, the melting of ice and snow is not

directly related to air temperature, but rather it is the circulation of air through the turbulent eddies near the glacier surface that regulates the majority of the atmospheric heat transfer. As a result, the melting of GIC is directly linked to atmospheric conditions and this makes them a sensitive indicator of climate change (Figure 1-4). Although GIC account for less than 1 % of the total land ice on Earth, they are one of the major contributors to GMSL rise and the largest contributor to GMSL rise during the 20th century (Gregory et al., 2013). The change in GMSL due to the addition or removal of water from the ocean is referred to as barystatic sea level change. Deformational and gravitational effects are not included when calculating barystatic sea level change. Water mass contribution to sea level change is measured by its sea-level equivalent (SLE) which is the mass of water (liquid, ice, or vapor) converted to volume using a density of $1000\,\mathrm{kg\,m^{-3}}$ and then dividing that volume by the surface area of the present-day ocean, $3.625 \times 10^{14}\,\mathrm{m^2}$. Therefore, in order to cause a 1 mm rise in GMSL it would require the addition of 262.5 Gt of water mass to the ocean (IPCC, 2013).

Since fluids cannot support a shear stress, the free surface of any fluid at rest will always lie perpendicular to the direction of any external forces applied to it. If it were not perpendicular, it would flow until it was. As a result, the equilibrium ocean surface is perpendicular to the Earth's gravity field at every point over the ocean. This surface is called the geoid (Figure 1-1). However, because the ocean is never in equilibrium due to a variety of perturbations (e.g. ocean circulation, wind, tides, and earthquakes), the geoid is a hypothetical surface. Any process that leads to a redistribution of mass, such as the movement of water and ice during glacial cycles, will therefore influence the height of the geoid. These changes in the distribution of mass on the surface and inside the Earth result in non-uniform changes to the geoid and thus non-uniform changes in the ocean surface (Milne, 2014).

Bodies of ice, either portions of an ice sheet or GIC, exert a gravitational pull which attracts surrounding ocean. When the ice begins to melt the gravitational attraction is reduced and the associated geoid high will diminish in amplitude. As a result, the RSL for a particular location will vary with distance from the ice body

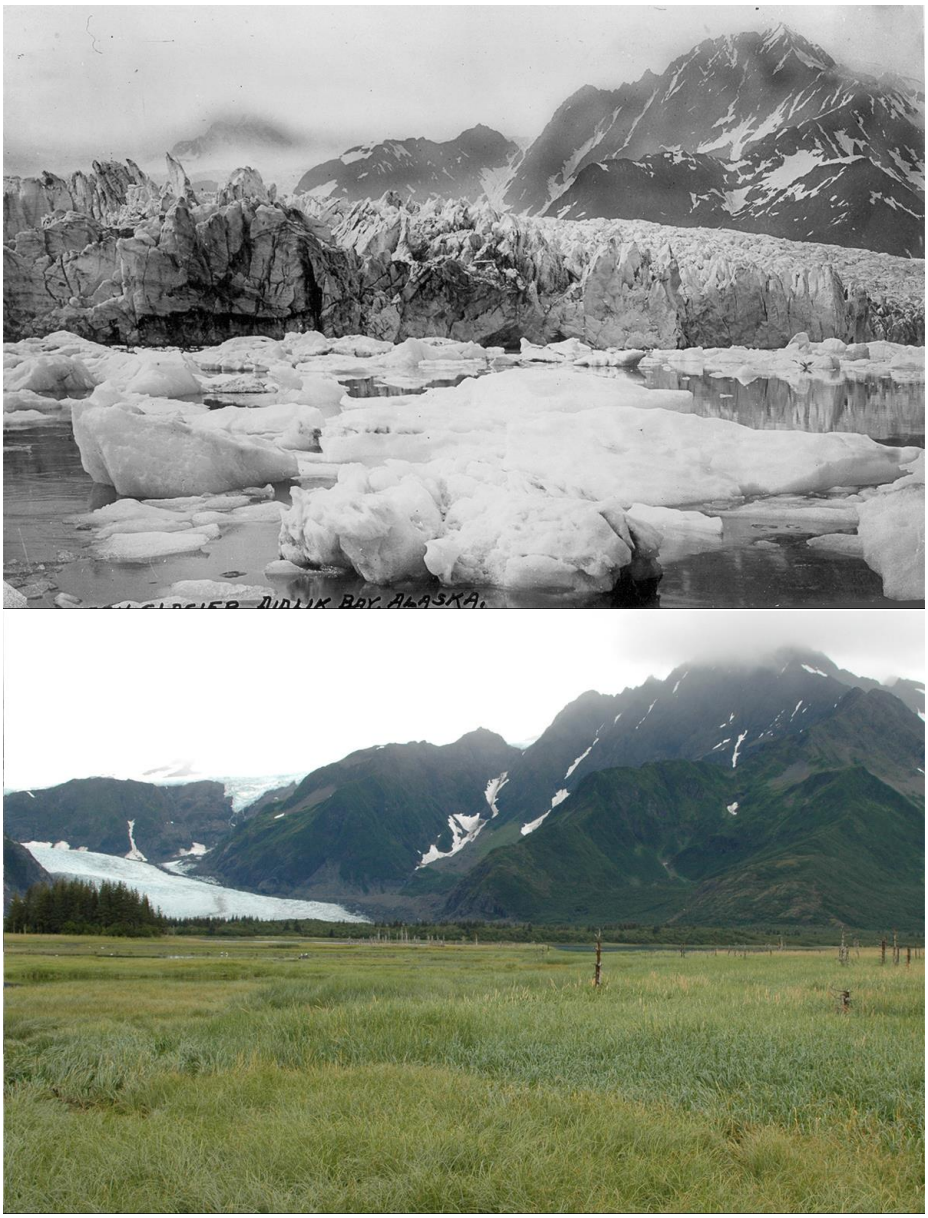

Figure 1-4. Pedersen Glacier, Alaska, USA. Picture on the top: photographed in the summer of 1917 (Pedersen, 1917). Picture on the bottom: photographed in the summer of 2005 (Molnia, 2005).

(Figure 1-5). Regions close to the source are referred to as “near-field" locations. Sea level in the near-field will fall due to the weakened gravitation attraction and the viscoelastic uplifting of the solid Earth. The “far-field" refers to regions that are at great distances (thousands of kilometers) from the center of the ice body. In these regions, barystatic sea-level rise, widening of the ocean basins, and crustal tilting due to hydro-isostasy dominate the RSL change (Milne, 2015). As a result, the redistribution of melt water mass is not uniformly distributed across the globe, but rather produces distinct spatial patterns of sea-level change referred to as sea-level fingerprints, which will be discussed further in section Section 1.4.

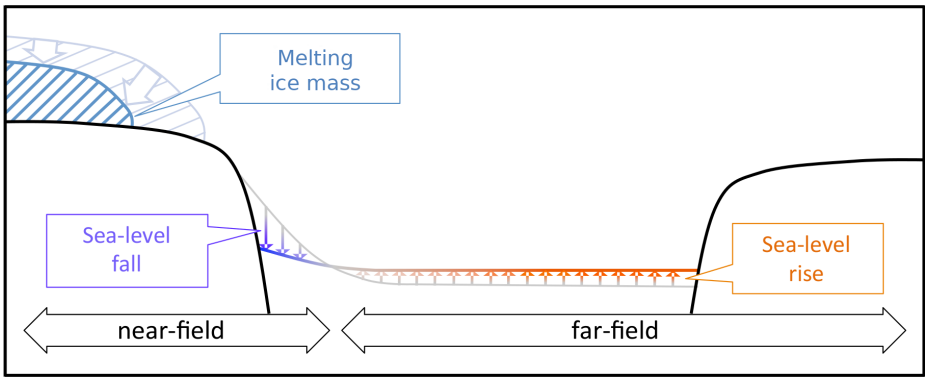

Figure 1-5. As the ice mass melts the RSL in the near-field will fall (blue arrows) due, in part, to decreased gravitational pull resulting in the redistribution of melt water across the global and the rise in sea level in the far-field (orange arrows). For clarity, changes in solid Earth are not depicted see Figure 1-2 (Botella, 2015).

There is also a rotational component of sea-level change associated with ice mass change. The rotation vector (direction and speed) of the Earth changes when mass is redistributed on the surface and the solid Earth is deformed. This change in the rotation vector induces height changes of both the Earth’s solid surface and the geoid, thus producing a change in RSL (Milne and Mitrovica, 1998).

1.2.1.2 Changes in ocean density

Earth’s ocean is a large complex body comprised of seawater with density varying from place to place due to non-homogeneous physical and chemical properties. The density of seawater is a function of temperature, salinity, and pressure. As a result, sea level

at a given location is dependent on these three factors. Changes in sea level due to changes in density are called steric; more specifically, thermosteric changes are caused by fluctuations in temperature and halosteric changes are caused by fluctuations in salinity.

Temperature and density have an inverse relationship. As the temperature of the water increases, the average space between the molecules increases resulting in lower density. It would then stand to reason that as water temperature decreases the space between the molecules decreases resulting in higher density, which is true, but only to a point. Pure water reaches its peak density at 4 °C, if it cools further it starts to become less dense as the molecules arrange themselves into a rigid open pattern which is less dense than liquid water, explaining why ice floats. Due to it's large mass and high heat capacity, Earth's oceans are capable of storing huge amounts of energy. Given an equivalent increase in temperature, the oceans are capable of storing 1000 times as much energy as the atmosphere. Between 1971–2010 the ocean accounted for ∼93 % of the increase in Earth's energy inventory, with ∼64 % of the total being accounted for in the upper (0–700 m) ocean. Heat stored by land, atmosphere, and melted ice account for the remaining energy change (Rhein et al., 2013). This warming of the ocean has resulted in sea-level rise at both global and regional scales with thermal expansion currently the predominant cause of GMSL rise.

Salinity, on the other hand, has a direct relationship with density. As the level of salinity increases, the density of the water will also increase, and vice versa. Various events can contribute to a change in seawater salinity: for example, an influx in freshwater, either from melting ice bodies or river discharge will cause salinity to decrease and thus will result in a decrease in density and a sea-level rise. Conversely, the freezing of polar ice or evaporation will increase salinity and therefore increase density.

While wind is responsible for driving ocean currents in the upper 100 m of the ocean's surface, deep ocean currents which flow thousands of meters below the surface are driven by differences in ocean density. Because the density of ocean water is

controlled by temperature (*thermo*) and salinity (*haline*), this process is referred to as thermohaline circulation. Warm surface water driven by wind such as the Gulf Stream travels towards the poles from the equatorial Atlantic Ocean. As this water moves towards higher latitudes it becomes more dense due to lower air temperatures and increases in salinity due to evaporation and the formation of sea ice. As a result, this colder, denser water downwells (sinks) to the ocean basins. In the North Atlantic this is called the North Atlantic Deep Water. This water eventually upwells (rises) in the Antarctic, Indian, and North Pacific oceans where it begins the cycle again. Because of this circulation, steric sea-level implicitly includes a dynamic component which can affect global and regional sea level (Figure 1-6).

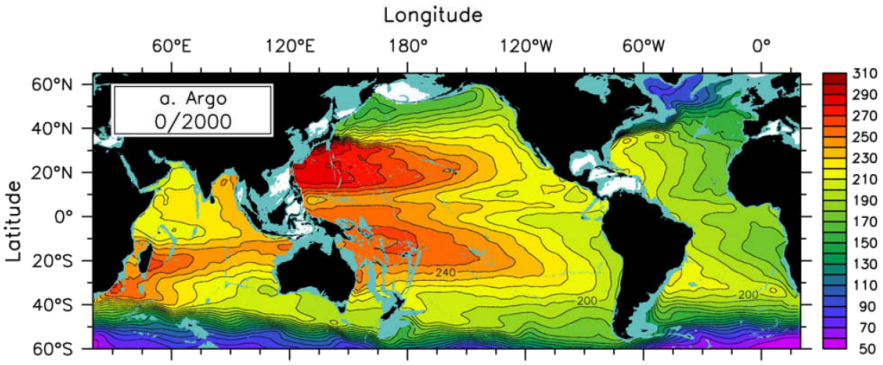

Figure 1-6. Steric height (dynamic cm) of the ocean surface relative to 2000 dbar from the 2004-2008 Argo mean (Roemmich and Gilson, 2009).

1.3 Sea level projections

Sea-level projections have traditionally focused on global mean change. Recently however, attention has been shifting more towards regional sea-level change which can deviate significantly from the global mean. In order to construct the scenarios for regional changes in sea level several components need to be combined. Figure 1-7 show a schematic of the different components that go into computing regional projections. A coupled climate model provides the majority of the data used to calculate the land ice as well as the steric contributions. These climate models use Representative Concentration Pathways (RCPs) which describe different climate scenarios of possible

future greenhouse gas emissions, these will be discussed further in Section 1.3.1. The land ice is divided into two components: the large ice sheets of Greenland and the Antarctica, and the smaller GIC. Once the location and magnitude of all the land ice mass is defined, the local sea-level fingerprint resulting from the melting land ice can be computed using a sea-level model. Global mean thermal expansion data and local RSL anomalies resulting from variations in temperature and salinity are used to compute the spacial pattern of the steric contribution. The response of the solid Earth due to ice mass changes after the last glacial maximum is still present today, therefore the spacially varying field of GIA must also be added to the other contributions.

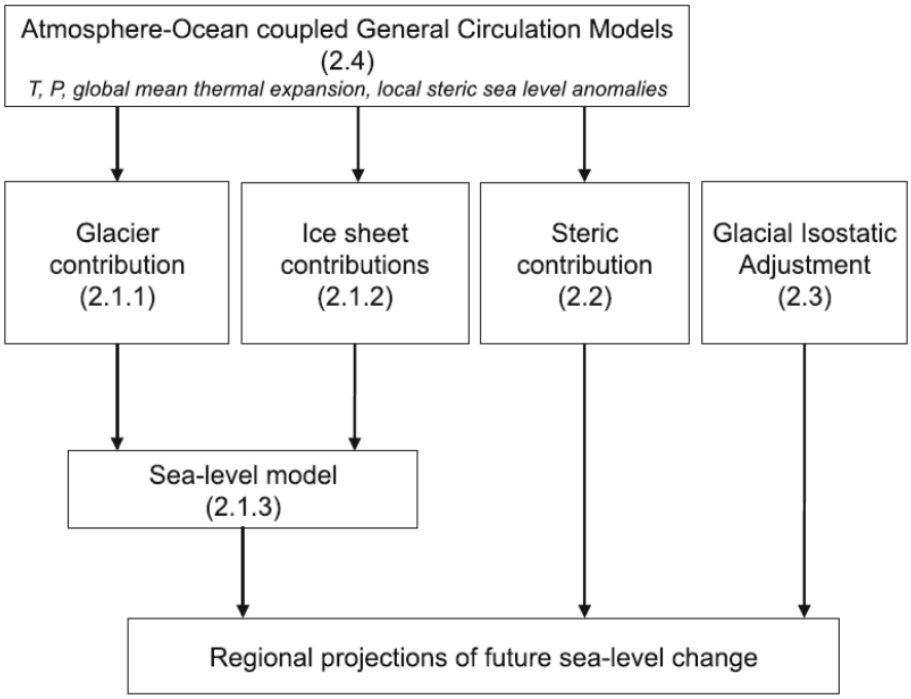

Figure 1-7. A schematic showing the different components used to project regional sea-level change. Temperature (T) and precipitation (P) are provided by the global climate models and are used to calculate the contribution from land ice and the steric contributions of global mean thermal expansion and local sea-level anomalies caused by temperature and salinity variations. Historic ice mass changes in the form of GIA must also be taken into account (Slangen et al., 2012).

Figure 1-8 shows individual spacial plots for each of the different components used in computing regional sea-level. In these series of plots the values are averaged over

the period of 2081-2100 relative to the reference period 1986-2005. In Figure 1-8a and Figure 1-8b the contribution of GIC and ice sheets is shown. These values were obtainted using the WRCP Coupled Model Intercomparison Project phase 5 (CMIP5) climate model for RCP4.5 and RCP8.5 respectively. Figure 1-8c and Figure 1-8d show the contribution of the steric and the ensemble mean dynamic topography for the two RCP scenarios from the same climate model. In addition, these two figures also include atmospheric loading (AL) which is not explicitly accounted for in coupled climate models. In Figure 1-8e the dynamic ice sheet contribution is shown, which was isolated in the study by Slangen et al. (2014) and made scenario independent as there were insufficient model results at that time to include in their analysis. Figure 1-8f is independent of the climate scenario and shows the effects of groundwater depletion. Figure 1-8g shows the effect of GIA which is also independent of the climate scenario. Additional information and analyses of these results can be found in Slangen et al. (2014).

1.3.1 Representative concentration pathways

The Fifth Assessment Report of the Intergovernmental Panel on Climate Change (IPCC AR5) introduced four radiative forcing scenarios representing future greenhouse gas concentration trajectories referred to as RCPs. Each of the RCPs refers to a particular scenario that includes a time series of emissions and concentrations of anthropogenic greenhouse gases. The four RCPs represent a possible range of radiative forcing by the end of the 21st century relative to pre-industrial ($\sim$1765 CE) levels with values of 2.6, 4.5, 6.0, and 8.5 $\mathrm{W\,m^{-2}}$ are referred to as RCP2.6, RCP4.5, RCP6.0, and RCP8.5, respectively (Figure 1-9).

RCP2.6 can be described as a "mitigation" scenario where radiative forcing peaks before 2100 at approximately 3 $\mathrm{W\,m^{-2}}$ and then declines to approximately 2.6 $\mathrm{W\,m^{-2}}$ by 2100. RCP4.5 and RCP6.0 are "stabilization" scenarios where the radiative forcing stabilize at approximately 4.5 and 6.0 $\mathrm{W\,m^{-2}}$ respectively after 2100. RCP8.5 is a "business as usual" scenario where radiative forcing is greater than 8.5 $\mathrm{W\,m^{-2}}$ by 2100 and continues to rise well after (IPCC, 2013).

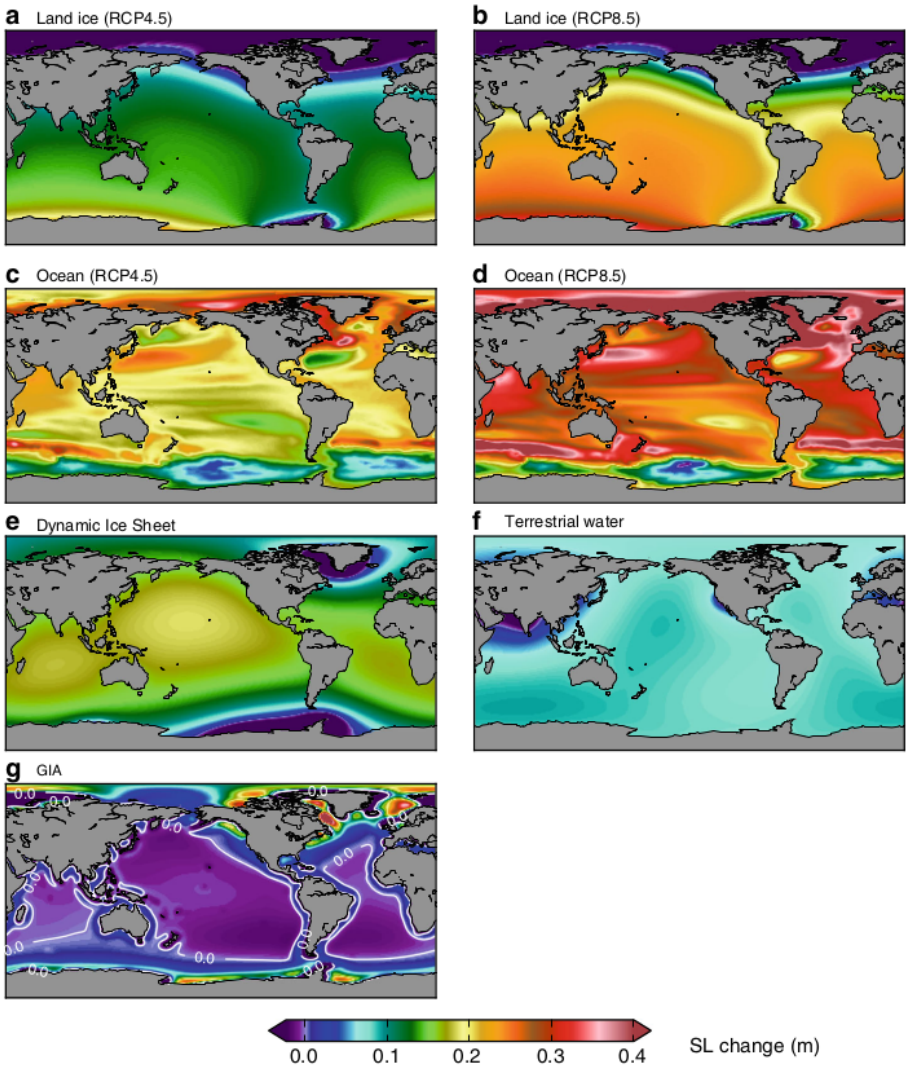

Figure 1-8. Projections of the time averaged sea-level change (m) over the period of 2081-2100 relative to the reference period 1986-2005; a) GIC and ice sheet surface mass balance using RCP4.5, b) GIC and ice sheet surface mass balance using RCP8.5, c) global steric and dynamic topography using RCP4.5 and AL, d) global steric and dynamic topography using RCP8.5 and , e) ice sheet dynamics, f) groundwater depletion, g) GIA. Note: e), f), and g) are independent of the climate scenario (Slangen et al., 2014).

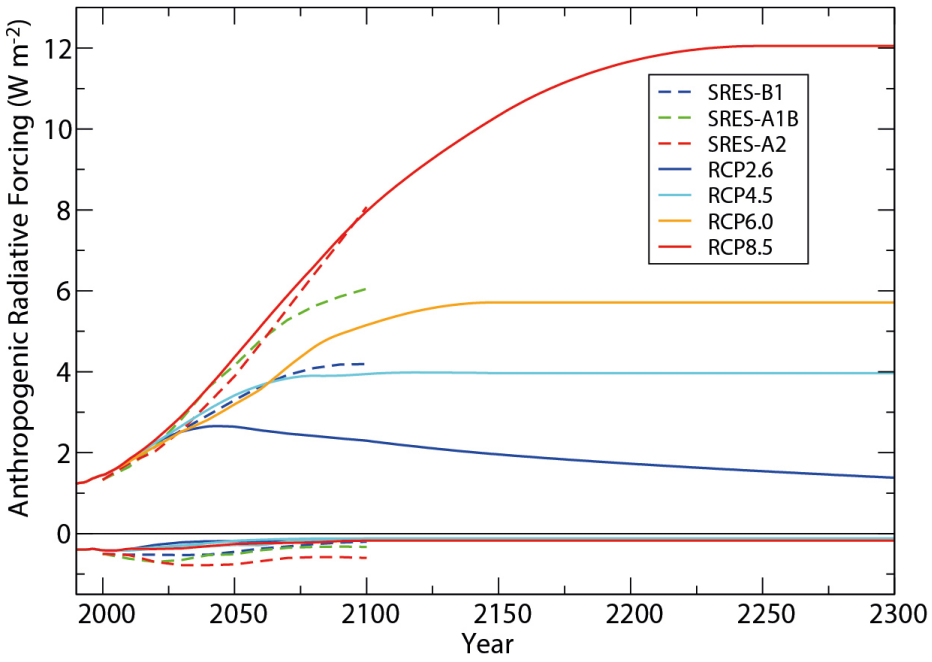

Figure 1-9. Time series of the total anthropogenic radiative forcing between 2000 and 2300 relative to pre-industrial (approximately 1765) levels for RCP scenarios and their extensions (continuous lines). Additional information can be found in Collins et al. (2013).

In this thesis I will be using the RCP4.5 scenario when determining glacier mass loss because it is a "middle of the road" scenario and the focus of this thesis is on the RSL response to a given scenario rather than the likelihood of one RCP scenario over another. That being said, the technique I use could be adopted for any of the RCP scenarios.

1.4 Modelling sea-level fingerprints

Over short time scales (decades to centuries), the rapid melting of glaciers and ice sheets results in distinct spatial patterns of sea level change (Figure 1-10). These patterns are referred to as sea-level fingerprints and can be used to understand past and project future changes in RSL. Over these same timescales, the viscous flow of Earth's interior is a small component of the total deformation of the solid Earth due to ice loading in most regions. Because of this, sea-level fingerprints normally do not include the viscous component and are computed using an elastic Earth model only.

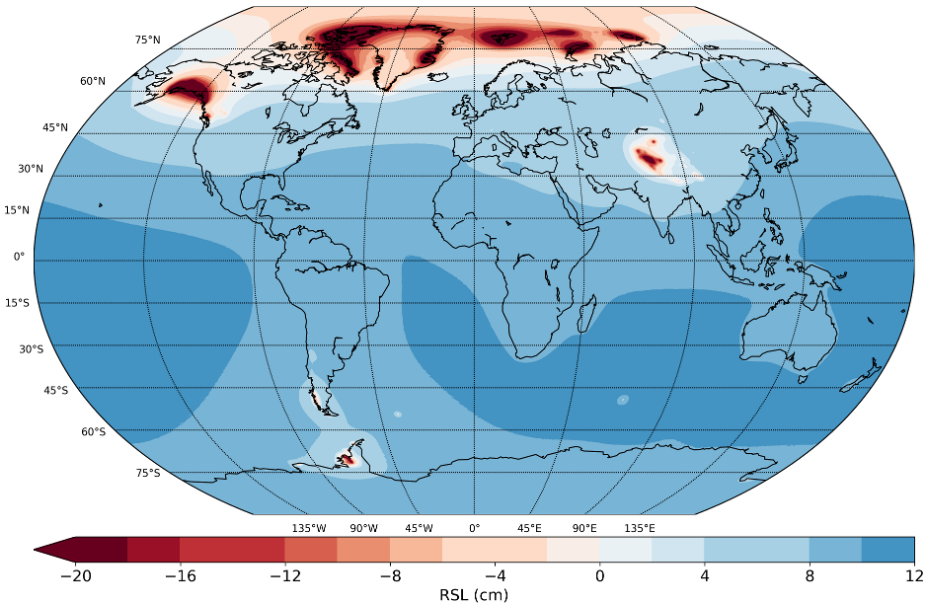

Figure 1-10. Global sea-level fingerprint projection for 2100 assuming an elastic Earth response and RCP4.5 based projected mass loss for GIC.

However, there is evidence that the glaciated regions of Alaska, Western Canada and US, and the Southern Andes are situated on top of mantle regions in which the local viscosity is several orders of magnitude lower than typical global mean values (Jin et al., 2017; James et al., 2009; Richter et al., 2016, respectivly). In regions where the viscosity is relatively low, the viscous component of deformation can be significant (Hay et al., 2017). Therefore, under these circumstances it is important to consider Earth models that take into account viscoelastic deformation which requires a method of inferring the mantle viscosity for a given region and constructing an Earth model based upon the results.

In this section, I outline the general methodology used in computing sea-level fingerprints. The underlying theoretical framework of this methodology is represented by the so-called "sea-level equation".

In 1976, Farrell and Clark presented a sea-level theory that accounted for both the deformation of the Earth and changes in the gravity field caused by mass changes in land ice. The equation that they introduced has became the basis for modeling sea-level variations due to land ice changes and is commonly know as the sea-level equation. The equation has since been refined and extended to include the changes

in Earth rotation (e.g. Milne and Mitrovica, 1998; Mitrovica et al., 2005) and is described in detail by Kendall et al. (2005).

Solving the sea-level equation ensures that the redistribution of meltwater includes the processes described above: earth deformation, changes in gravity and changes in Earth rotation. The sea-level equation has two primary inputs: a realistic model of the Earth (density, rheology) that can respond to surface loads, and a realistic ice loading history to force the model. Because the ocean load is both an input and an output it is solved for iteratively (Figure 1-11).

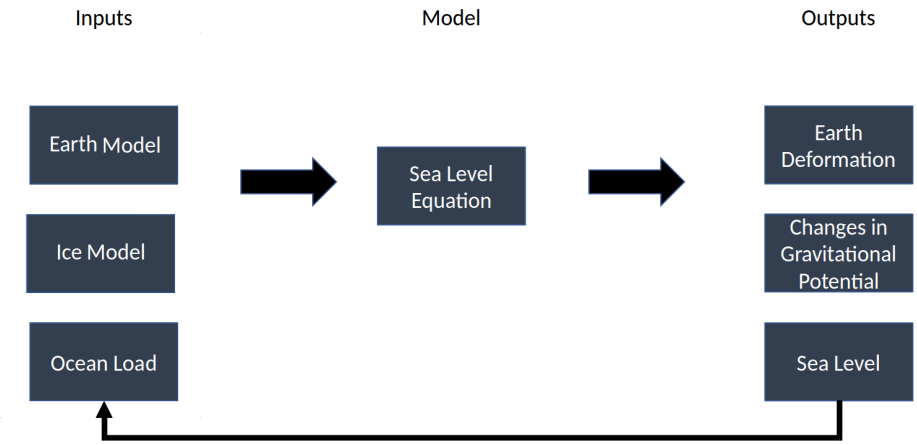

Figure 1-11. A flowchart outlining how the SLE is used to calculate changes in RSL. The ocean load is solved iteratively because it is both an input and output of the sea-level equation.

In following sections, the two primary inputs to the computer code that solves the sea-level equation are described: a model of ice extent changes (Section 1.4.1) and a model of Earth rheology (Section 1.4.2).

1.4.1 Modelling the ice

Ice models are created to provide the space-time evolution of ice extents. I make use of the Randolph Glacier Inventory 5.0 (RGI) to determine the area of the glaciers in the study regions. The RGI was initially created for use in the IPCC AR5. It is a complete global collection of digital outlines of glaciers and ice caps grouped into 19 first-order regions (Figure 1-12). While it does include the peripheral glaciers of

Antarctica and Greenland, it does not include the ice sheets. Most of the outlines were obtained from satellite imagery from 1999-2010 (Arendt et al., 2015). The strength of the RGI is its ability to handle many glaciers at once, rather than measure rates of area change on a glacier-by-glacier basis. For example, the RGI is well suited for estimating regional and global scale rate of glacier elevation and volume changes.

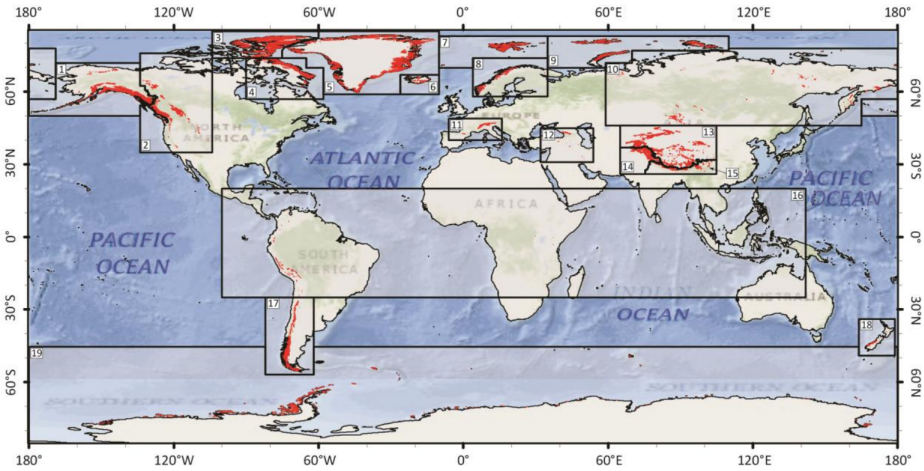

Figure 1-12. The 19 first-order regions in the RGI. This thesis will primarily be focused on (1) Alaska, (2) Western Canada and USA, and (17) Southern Andes. Additional information can be found in Arendt et al. (2015).

1.4.2 Modelling the Earth

When stress is placed on the Earth it exhibits both elastic and viscous behaviours. When force is applied to a material that behaves elastically, it will instantaneously deform, then once the stress is removed it will immediately return to its original shape. When stress is applied to a material that behaves viscously it will undergo transient, permanent deformation. This deformation may either be linear or non-linear. A material that exhibits both elastic and viscous behaviours is called a viscoelastic material and it will have both instantaneous and transient deformation when a force is applied to it. On the time scale of glacial cycles (∼100,000 years), the lithosphere behaves like an elastic body and the mantle behaves like a viscoelastic body. On timescales of ∼100 years, the entire solid Earth (except the fluid Outer Core) acts like an elastic body. The depth of the mantle's response depends upon the size of

the load, with the largest ice sheets resulting in deformation extending to the lower mantle (i.e. below the 670 km depth seismic velocity discontinuity).

In order to apply the sea-level equation, a spherical Earth model must be used. As the name implies, an elastic Earth model assumes that the Earth will behave elastically and therefore the viscosity structure of the Earth's mantle does not need to be known. On the other hand, when using a viscoelastic Earth model it is necessary to define the viscosity structure of the Earth's interior. The viscoelastic model may consist of hundreds of layers in order to capture elastic and density variations with the lithosphere being assigned a very high viscosity (1×10^{43} Pa) to simulate an elastic response. However, due to uncertainties in the structure of the Earth's interior, the viscosity structure of the mantle is normally crudely divided into two layers, one for the upper mantle and the other for the lower mantle, although some models may have more. The viscosity structure is often treated as a free parameter so that it may be inferred when fitting GIA-related data (e.g. RSL).

Traditionally, GIA modelling has assumed a 1D Earth model where variations in material only occur in the radial direction (with depth), and that the rheology of the mantle is linear (i.e. Maxwell viscoelastic). Although it is now known that the mantle viscosity varies laterally as well as with depth and that the mantle rheology may potentially be linear, non-linear, or a composite of both, using a more simplified model has facilitated the computation of Earth deformation via the sea-level equation. In more recent years, however, improvements in computational power have allowed for the introduction of more complex 3-D Earth models that can incorporate lateral variation in both the thickness of the lithosphere and in the viscosity of the mantle, as well as linear, non-linear, composite, and/or transient mantle rheologies (Whitehouse, 2018).

1.5 Aim of this thesis

As indicated above, future changes in RSL will be influenced by different processes. Therefore, any attempt to quantify future sea-level change should account for these

different processes (e.g. Slangen et al., 2012) as the accuracy of a given sea-level projection depends on the accuracy of the individual components of the net signal.

The primary goal of this thesis is to determine if the viscosity of the Earth's mantle plays a significant role in the computation of sea-level fingerprints. Most current sea-level projection studies have used fingerprints computed using an elastic Earth model. So my aim is to assess the accuracy of assuming an elastic Earth model when computing the fingerprint due to GIC changes. Specifically, I focus on regions where the mantle viscosity is orders of magnitude lower than the global average (Alaska, Western Canada & USA, and the Southern Andes) and compare sea-level fingerprints computed using an elastic Earth model to those computed using a 3-D viscoelastic Earth model.

2

Sea-Level Fingerprint Modelling

2.1 Introduction

For the past two millennia, up until the 20th century, there has been relatively little change in GMSL (Masson-Delmotte et al., 2013; Kopp et al., 2016) and during this period of relative sea level stability, coastal regions became attractive locations for human settlement. Fertile land, mild climate, and access to the oceans for both resources and transportation lead many of these settlements to become hubs for trade and commerce (Griggs, 2017). During the 20th century and into the 21st, major coastal cities continued to expand with eight of the world's largest cities on the coast having a cumulative population of just over 200 million. Of the twenty-five largest cities in the world, eighteen are coastal and have a combined population of 357 million people, almost 5% of the world's population (Griggs, 2017). However, contemporary

climate change has made settlements in coastal lowlands particularly vulnerable to sea-level rise, stronger and more frequent storms, and other seaward hazards.

Predicting sea-level rise is one of the great scientific problems of our time. The estimation of future GMSL rise is a non-trivial task and estimating local and regional sea level change is even more challenging where the vertical movement of either the ocean or land surface along any coast can cause (relative) sea-level change. A variety of processes may drive changes in the height of the ocean floor and ocean surface, and the combination of these processes produces a complex pattern of sea level change that varies through time as the relative contribution of each process often changes. While the global average change provides a useful single value which reflects the contribution of multiple processes and does represent a good estimate of sea level change at many coastal locations, various regional processes that produce a strong signal can result in large departures from the global average value (Church et al., 2013). As a result, predicting sea level at the regional scale requires an in-depth understanding of numerous physical processes that have a range of spacial scales and response times.

Around the world, glaciers and ice sheets are losing mass and retreating (Hartmann et al., 2013; Rhein et al., 2013). Observations since 1850 show that, on a global scale, the rate of glacier mass loss in the early 21st-century is without precedent for the observation period (and potentially for all recoded history) (Zemp et al., 2015). The melting of ice sheets and glaciers produces a complex pattern of sea level change due to the resulting solid Earth deformation and changes to the geopotential (Farrell and Clark, 1976). When these changes happen on decadal to centennial time scales the resulting solid Earth response is dominantly elastic and so the non-elastic (viscous) component is commonly ignored. The modelled spatial patterns in relative sea-level change associated with these short-term changes in ice mass are often termed "sea-level fingerprints" (e.g. Mitrovica et al., 2011).

The assumption of an insignificant contribution of the non-elastic signal to sea-level fingerprints was recently addressed in a paper focusing on mass loss of the Antarctic ice sheet (Hay et al., 2017). The viscosity of the Earth's mantle is known to

be several orders of magnitude lower than that of the global average in this region (e.g. Whitehouse et al., 2019). Hay et al. (2017) concluded that the viscous component of the response was significant and so should be included when computing sea-level fingerprints. Recent studies however have provided evidence that the glaciated regions of Alaska, Western Canada & USA, and the Southern Andes are located overtop of mantle regions where the local viscosity is several orders of magnitude lower than typical global mean values (Jin et al., 2017; James et al., 2009; Richter et al., 2016, respectivly). Therefore, in these regions it may be important to consider Earth models that take into account viscoelastic deformation.

While most current sea-level projection studies have used fingerprints computed using an elastic Earth model, in this study we explore the impact that lower than average mantle viscosity plays in the computation of sea-level fingerprints and assess the accuracy of assuming an elastic Earth model when computing the fingerprint. Specifically, we focus on regions where the mantle viscosity is orders of magnitude lower than the global average (Alaska, Western Canada & USA, and the Southern Andes) and compare sea-level fingerprints computed using an elastic Earth model to those computed using a 3-D viscoelastic Earth model.

2.2 Model description

In this study our results were generated using a numerical finite-volume formulation of the surface loading process (Latychev et al., 2005). This formulation assumes a Maxwell (steady state) rheology and is for a spherical tetrahedral grid in which the resolution is variable with the greatest variability near the surface of the Earth model. The lateral resolution varies from ∼15 km to ∼60 km at the core-mantle boundary. Immediately beneath the surface, the depth resolution is ∼12 km, compared to ∼50 km immediately above the core-mantle boundary. Using a specific surface (ice) loading history and Earth density and viscoelatic structure, this model computes several observables, including RSL and the present-day rates of vertical land motion (VLM) and geoid change.

The algorithm used in the 3-D Earth model simulations presented here is based on the theory described in Kendall et al. (2005) which includes the GIA-induced changes in Earth rotation (Milne and Mitrovica, 1998; Mitrovica et al., 2005). This theory describes how to solve the generalised sea-level equation, which can be written,

$$\Delta SL(\theta, \psi, t) = \left(\frac{\rho_I}{g}\Phi_I{}^* I\right) + \left(\frac{\rho_W}{g}\Phi_O{}^* \Delta SL\right) + C_{SL}(t) \tag{2.1}$$

where θ is the co-latitude and ψ is the longitude of the sea-level change. t is the time relative to some reference time, and g is the gravitational acceleration. ρ_I and ρ_W are the density of ice and water, respectively. I is a function that defines changes in grounded ice thickness and ΔSL is a function that defines changes in ocean depth. Φ is a sea-level Green's function that, when convoluted in space and time (represented by *) with a surface load, defines ocean depth change contributed by that load history, with I and O subscripts indicating that the spatial convolutions are performed over the area of ice and ocean, respectively. The final term $C_{SL}(t)$ represents a spatially uniform height shift of the ocean surface and it is used to ensure the conservation of ice-ocean water mass.

In order to use this model, two primary inputs must be defined: a realistic space-time evolution of grounded land ice to force the model and a realistic model of the Earth that defines the density and rheology which can respond to surface loads. The ice and Earth models used in this study are detailed below.

2.2.1 Ice models

In this study we created ice models for each of the 19 first order regions in the RGI (Figure 1-12). The RGI provides the area (Figure 2-1) for the GIC in each of the regions and then we apply the region-specific thickness-area scaling function of Huss and Farinotti (2012) which calculates the mean thickness of each glacier in a region using:

$$\bar{h} = cS^{\gamma} \tag{2.2}$$

Where $\bar{h}$ is the mean thickness, S is the area of the glacier, and c and γ are constants specific to each region in the RGI.

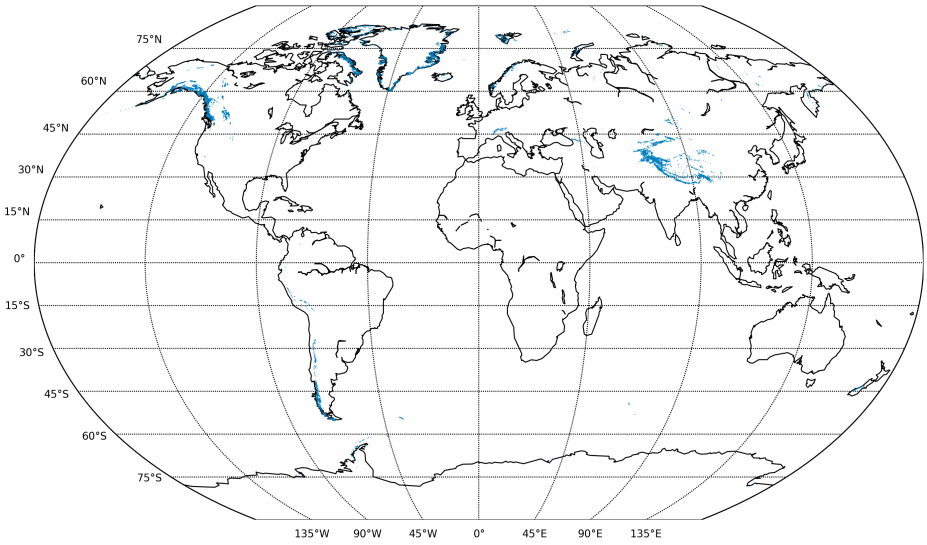

Figure 2-1. The spacial distribution (blue) of glaciers and ice caps as defined in the RGI.

In order to apply a mass loss history to our ice model for all 19 regions in the RGI we use the decadal RCP4.5 mass loss projections provided by Huss and Hock (2015) for the period 2010-2100 CE with a net barystatic sea-level change of 10.8 cm. By using the decadal mass loss projections we were able to emulate not only the thinning of the GIC but also the lateral shrinking of the ice extent to produce a non-linear GIC evolution scenario.

In order to achieve this we iterated over each of the decadal timesteps and calculated the required amount of uniform ice thickness (based on areal extent) that would need to be removed to equal the projected SLE mass loss for that decade using a tolerance of $\pm 1\,\%$. We then subtracted this amount from the previous timestep so that the lateral changes of the previous timesteps were incorporated in the current timestep. We then applied a spacial Gaussian filter to each timestep (using NumPy 1.16.1 Multidimensional Gaussian filter) with a standard deviation of 3.5 to spatially smooth the ice thickness distribution. This was done to reduce the numerical artifacts associated with the Gibb's effect when we represent the ice distribution as a truncated series of spherical harmonic functions. This process was applied individually to each

of the 19 first order regions in the RGI.

From these results we were also able to produce a linear mass loss evolution scenario for each region by simply subtracting the extent at 2010 CE from the extent at 2100 CE (Figures 2-2 and 2-3).

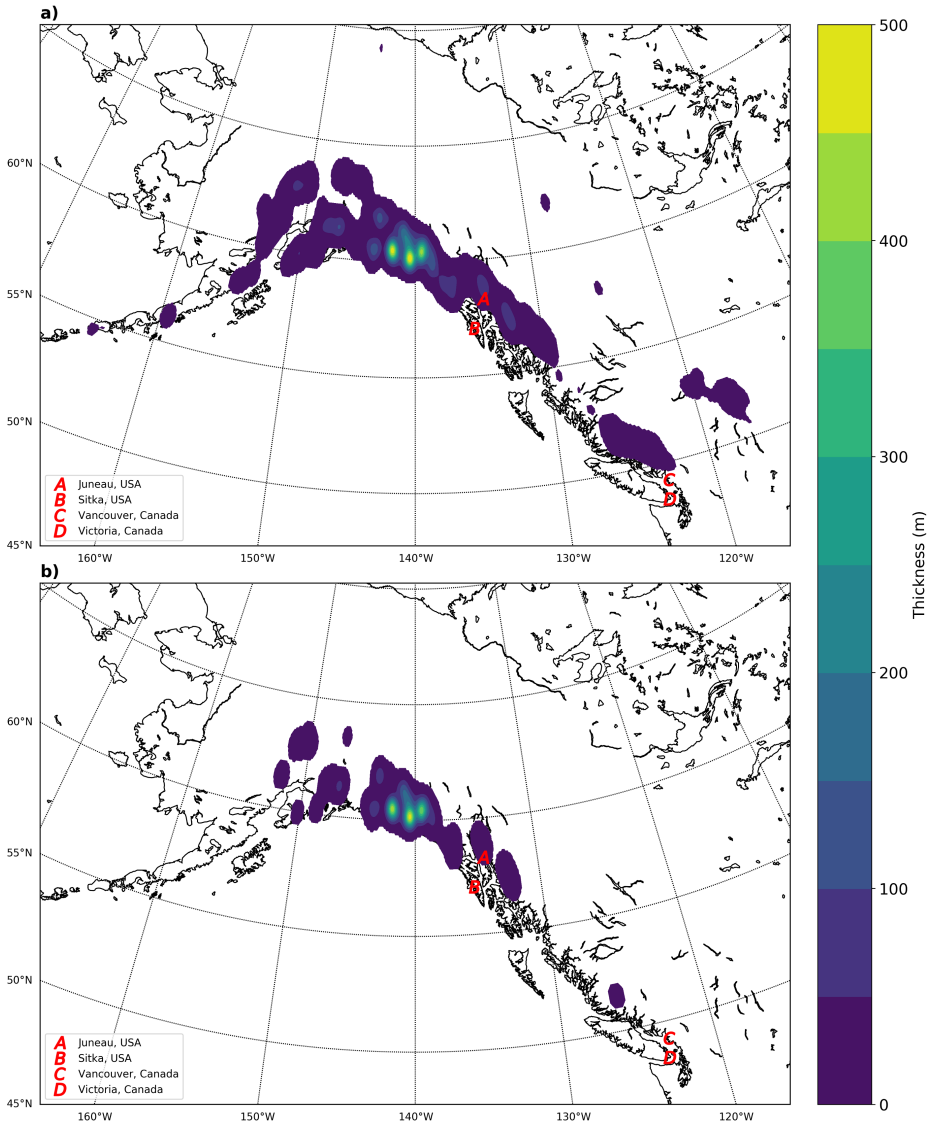

Figure 2-2. The extent and thickness of the ice models for the Alaska and Western Canada & USA regions at 2010 (a) and 2100 (b).

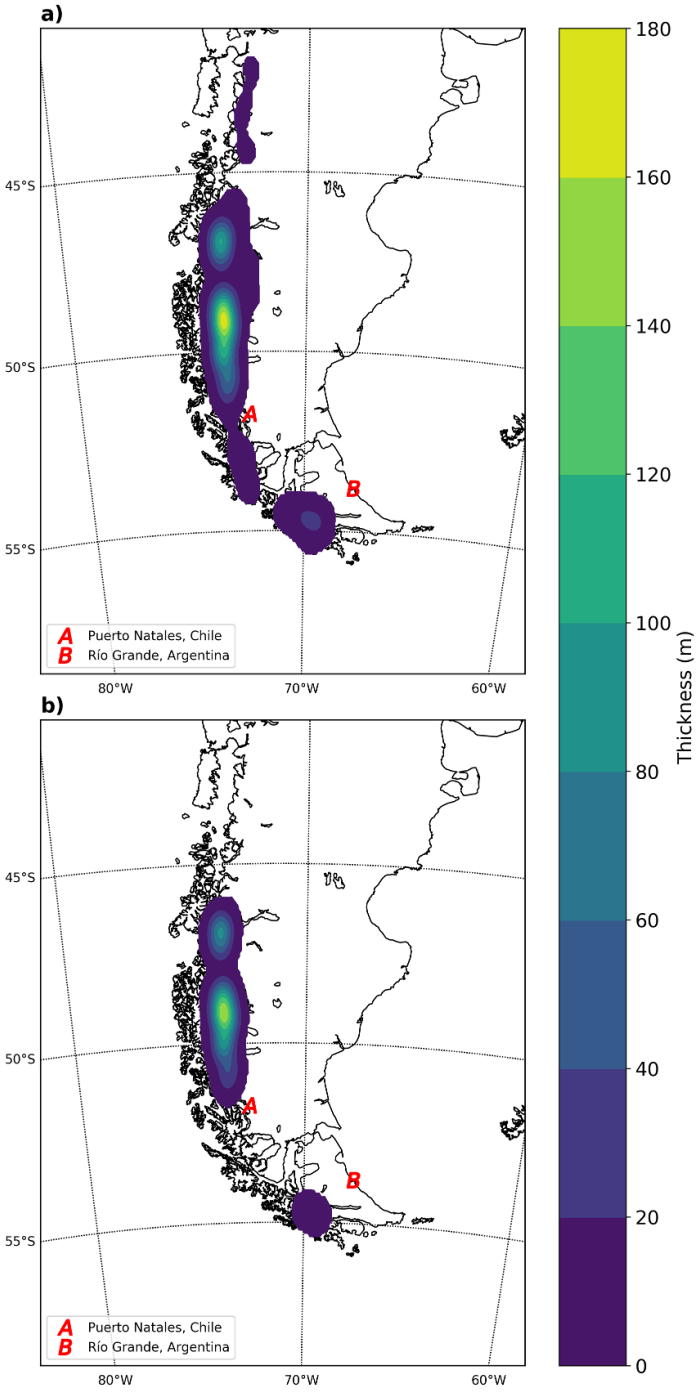

Figure 2-3. The extent and thickness of the ice model for the Southern Andes region at 2010 (a) and 2100 (b).

2.2.2 Earth model

The density and elastic properties of our Earth model are defined using the seismic Preliminary Reference Earth Model (Dziewonski and Anderson, 1981). Due to large uncertainty in our knowledge of the viscosity structure of the Earth, the viscosity structure is, unless otherwise stated, defined by only three parameters: the first is an outer shell of high viscosity (1×10^{44} Pa s) which is used to simulate an elastic outer shell (the lithosphere), the second is an isoviscous upper mantle region which extends from the base of the lithosphere to a depth of 671 km, and third, an isoviscous lower mantle region that extends from 671 km to the core-mantle boundary (2885 km). The values used to define the viscosity vary depending on the region detailed below resulting in an Earth model where the internal viscosity structure varies not only with depth but laterally as well. In contrast, the surface features of the Earth model (e.g., ice extent, topography) vary as a function of time and geographic position.

In defining global-scale viscosity structure we assign a lithospheric thickness of 96 km, an upper-mantle viscosity of 5×10^{20} Pa s, and a lower-mantle viscosity of 1×10^{22} Pa s. While these values are considered to be a good approximation of global average viscosity structure (Peltier, 2004), given the short time period of our model simulation, the use of other global average viscosity structures could be substituted in without impacting the results.

For RGI region 1 (Alaska), Jin et al. (2017) use measurements from Ice Cloud and Land Elevation Satellite (ICESat), global positioning system (GPS), and Gravity Recovery and Climate Experiment (GRACE) to estimate an optimal density for Alaskan glaciers. They inferred a best fit Earth model for the GIA effects in Alaska by fitting the model uplift rates with GRACE and GPS residual signals. They concluded on a best fit three-layer Earth model consisting of a lithospheric thickness of 60 km, a 110 km thick asthenosphere with a viscosity of 2×10^{19} Pa s, and a sub-asthenosphere mantle with a viscosity of 4×10^{20} Pa s. The lateral extent of these viscosity values at the model Earth surface is shown in red in Figure 2-4. In order to constrain the lateral extent of the low viscosity region we define a surface area that is roughly similar to

the region to which the Jin et al. data refers. We then define the viscosity structure in this region using the values defined in those studies. Note that the extent of this region decreases with depth to ensure that the proportion of this region relative to the global area at a given depth remains constant.

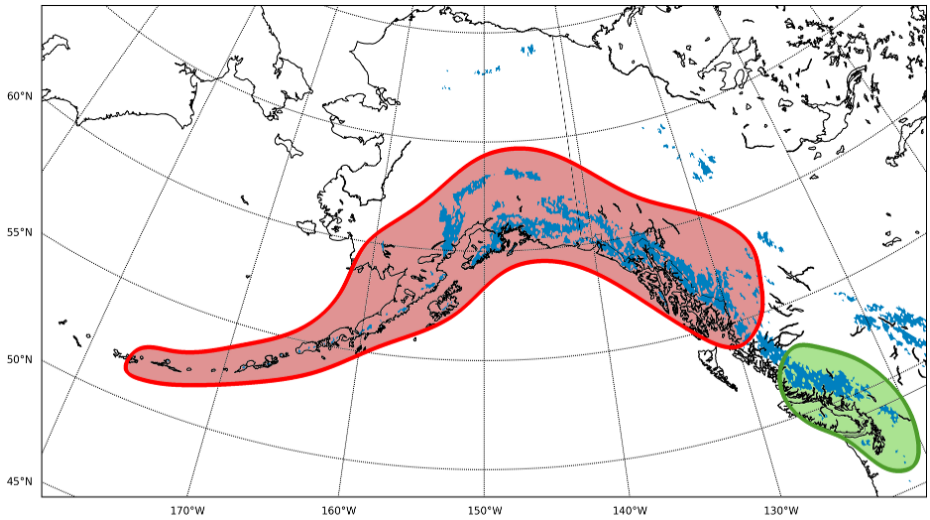

Figure 2-4. The lateral extent of low viscosity zone for Alaska (red) and Western Canada & USA (green). Lateral extent of ice as defined in the RGI shown in blue.

For RGI region 2 (Western Canada & USA), we are interested only in the area adjacent to southwestern British Columbia as this is where GIA studies have inferred low viscosity values: James et al. (2009) concluded that RSL observations from Vancouver Island can be fit equally well across a wide range of ansthenopheric thicknesses and viscosities. The Earth model with the lowest viscosity consisted of a lithospheric thickness of 60 km, a 140 km thick asthenosphere with a viscosity of 3×10^{18} Pa s, and a sub-asthenosphere mantle with a viscosity of 4×10^{20} Pa s. These results are supported by a more recent study that considered sea-level observations from a larger area in southwestern British Columbia (Yousefi et al., 2018). The lateral extent of these viscosity values at the model Earth surface is shown in green in Figure 2-4.

For the southern Andes region (RGI area 17), we adopted results from the analysis of Richter et al. (2016) who used observations from 43 geodetic Global Navigation Satellite System (GNSS) sites distributed over the Southern Patagonian Ice Field to analyze vertical and horizontal velocities of present-day crustal deformation. By

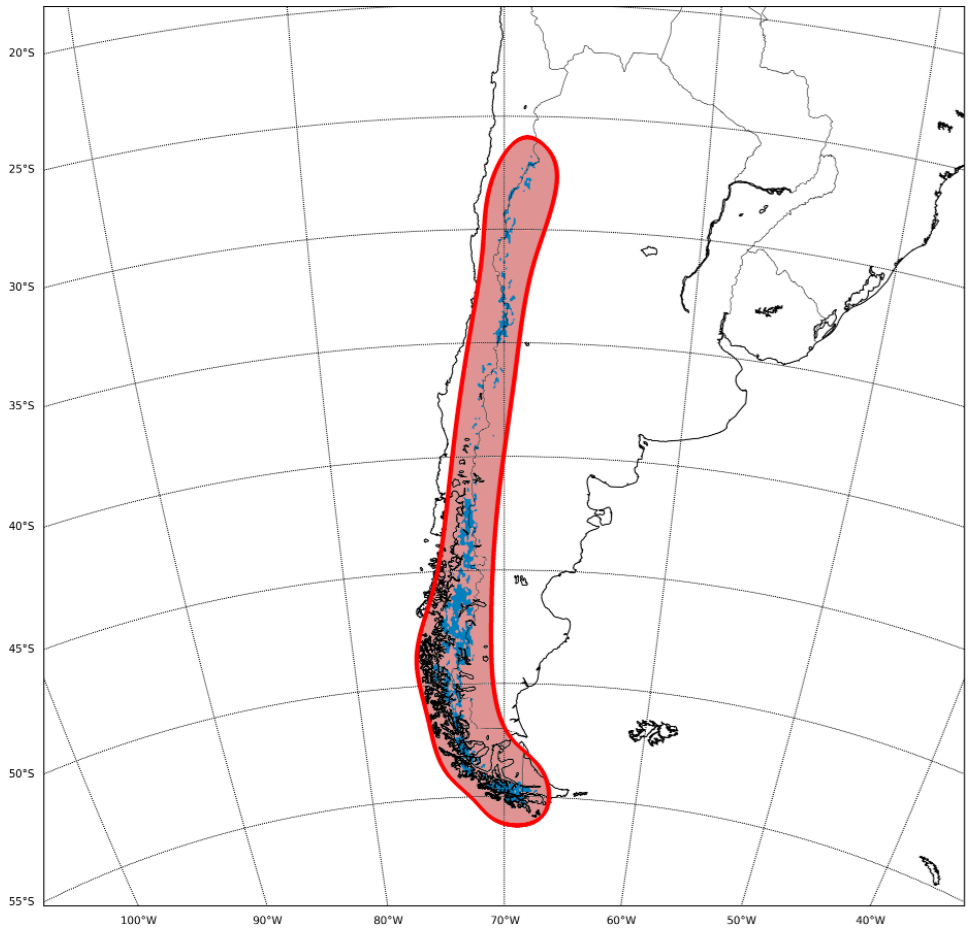

Figure 2-5. The lateral extent of low viscosity zone for the Southern Andes (red). Lateral extent of ice as defined in the RGI shown in blue.

applying an ice-load history that assumes a moderate present-day glacial mass loss, with slightly higher than present-day mass loss immediately following the Little Ice Age (LIA) maximum, Richter et al. concluded on a preferred Earth model consisting of a 36.5 km thick lithosphere and a sub-lithosphere mantle with a viscosity of 1.6×10^{18} Pa s. The lateral extent of these viscosity values at the model Earth surface is shown in red in Figure 2-5.

2.3 Results and discussion

Our goal is to quantify the potential signal of the viscous response from sea-level fingerprints computed for the three RGI regions introduced above. Results from our 3-D viscoelastic Earth model will be shown next to results from our elastic Earth model using the RCP4.5 GIC mass loss projections from Huss and Hock (2015).

Figure 2-6 shows global results for predictions based on the non-linear mass loss for all regions in the RGI. We plot the total sea level change from the start to the end of the study period. If the simulation were continued beyond the end of the study period, the impact of the viscous effects on the sea level change predictions would increase.

Firstly, we show the sea-level fingerprints calculated using our elastic Earth model (Figure 2-6a) and see the traditional GIC fingerprint where there is a sea level fall near the sources of the ice mass loss and a sea level rise in the far-field. We then consider the calculations based on our 3-D viscoelastic Earth model (Figure 2-6b) and can see that on a global scale the results look quite similar to the elastic results and so, in order to isolate the differences, we subtract the elastic results from the viscoelastic results (Figure 2-6c). In Figure 2-6c we see that in the far-field (locations that are on the order of 1000 km or more away from the ice load) the difference between the viscoelastic and elastic Earth models is negligible and in the intermediate-field (locations outside the boundaries depicted in Figures 2-4 and 2-5) the difference is generally less than 2 cm. However, in the near-field (the areas inside the boundaries depicted in Figure 2-4 and Figure 2-5), the difference in sea level change is significant

and can be several times larger than the global average (10.8 cm). The remainder of this section will focus on the signal in near-field regions only.

When we look at a close up of the viscoelastic minus elastic results for Alaska and Western Canada & USA (Figure 2-7b), there is a clear spacial pattern in this signal. Comparison of Figure 2-7b with the elastic results (Figure 2-7a) indicates that, in ice covered regions, the RSL change is less than that of the elastic case whereas peripheral to this area, the RSL change is greater. This pattern is somewhat intuitive when one considers that it reflects, in essence, a larger response of the solid Earth due to the faster response time of the low viscosity material. Because of the considerably lower mantle viscosity in these regions, the solid Earth responds faster than it otherwise would have over the same time period. As a result, the areas shaded in red show a greater sea level fall compared to the elastic case due to the considerable viscous uplift of the solid Earth. Similarly, the areas shaded in blue show a greater sea level rise as the peripheral bulge subsides more rapidly due to the viscous contribution.

In order to confirm that the difference in RSL is dominated by changes in VLM, we can look at the results for Alaska and Western Canada & USA in Figure 2-8 by removing the VLM (Figure 2-8b) from the total RSL signal (Figure 2-8a). In Figure 2-8c we can see that the remaining signal, changes in sea surface height (SSH), are an order of magnitude less than the VLM, thus confirming the dominance of this latter component signal.

In the time series plot of locations near the Alaska and Western Canada & USA regions (Figure 2-9), we see that including the viscosity structure in the Earth model, shown as a solid red line, makes a measurable difference compared to the elastic Earth model, shown as a solid green line. While the solid red line shows the total change in RSL, the dashed red line shows the change in RSL due to VLM only when using the viscosity structure in the Earth model. By subtracting the total from the VLM contribution we can determine change in RSL due to the changes in SSH.

At Juneau, USA, there is a difference of $\sim$74 cm in sea-level fall when compared to the elastic Earth model, meaning that the solid Earth is uplifting significantly faster over the 90 year period. In Sitka, USA, we see that, while the elastic Earth model

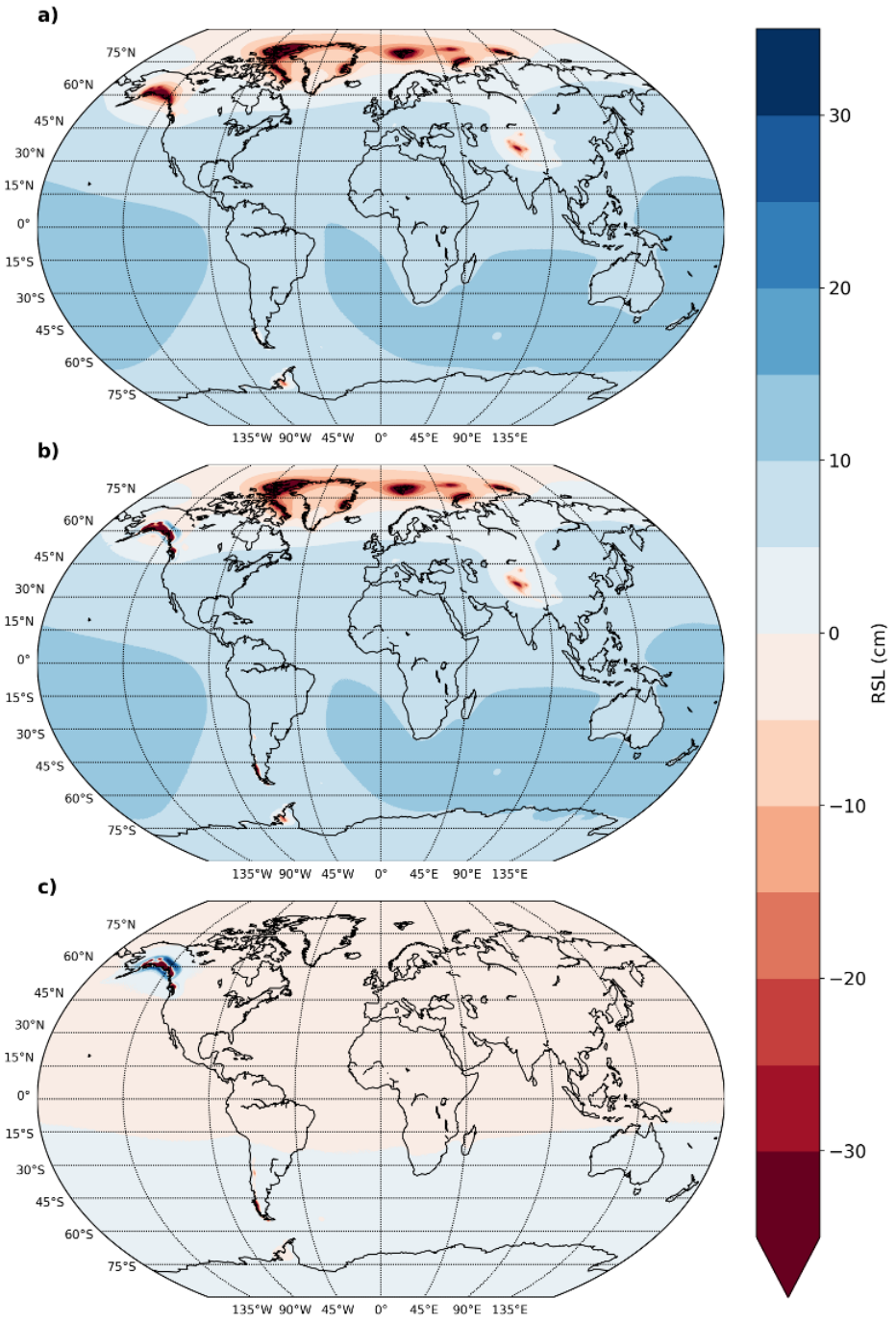

Figure 2-6. Global view of the difference (c) in RSL of the viscoelastic (b) and elastic (a) for all regions in the RGI.

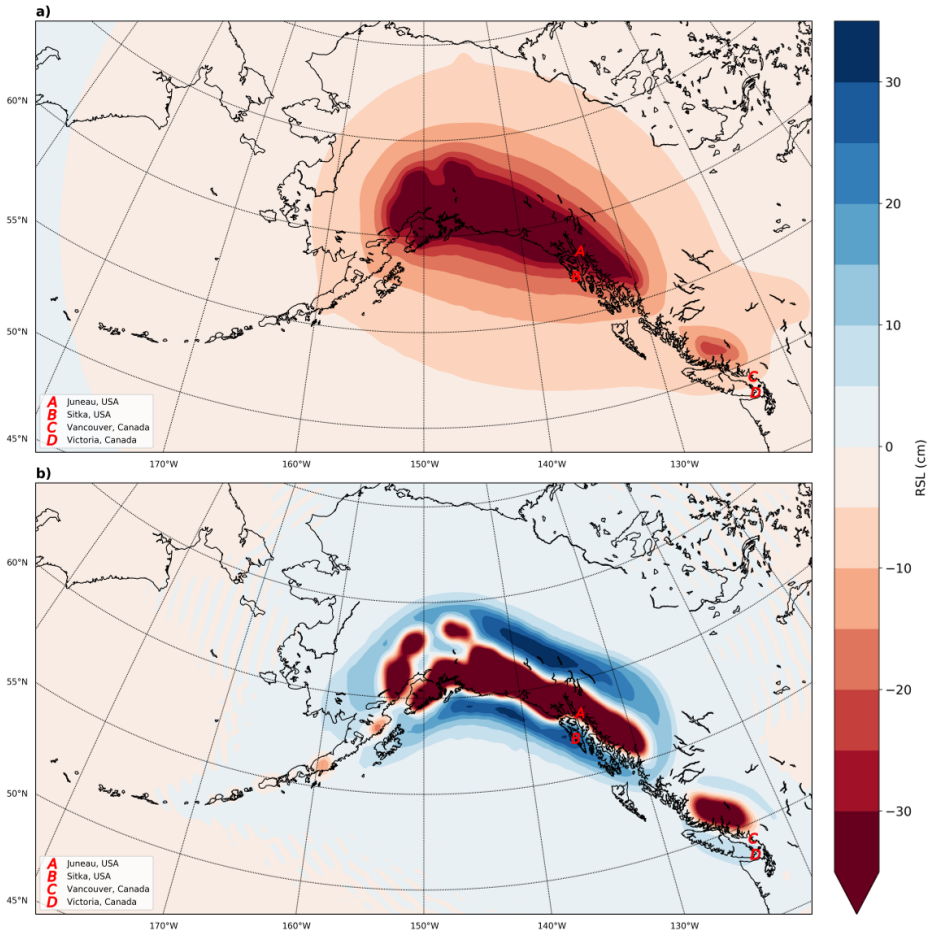

Figure 2-7. (a) The RSL elastic Earth model results for the Alaska and Western Canada & USA regions at 2100 CE. (b) The difference in RSL between the viscoelastic and elastic Earth models for the same regions and period.

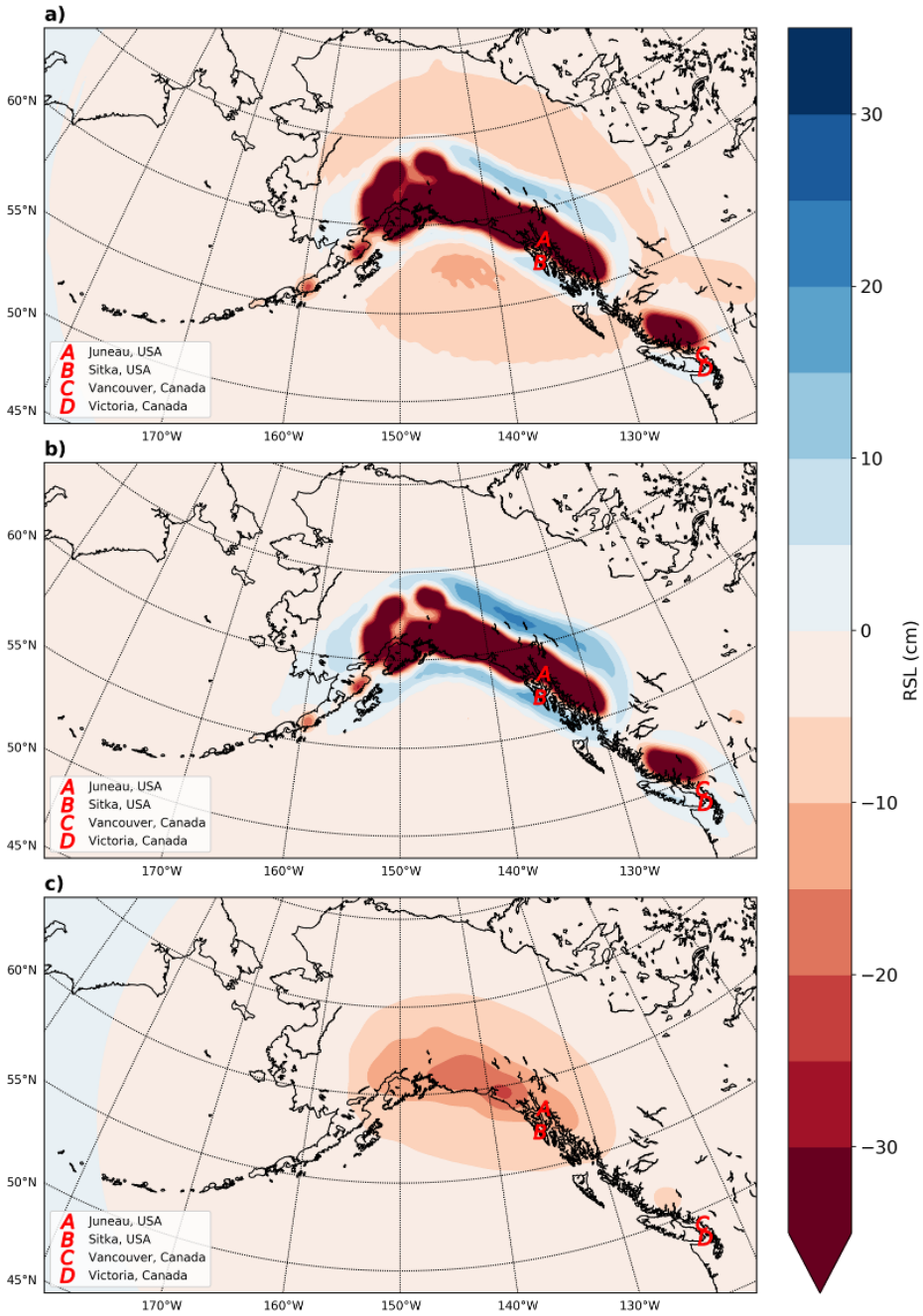

Figure 2-8. (a) The total change in RSL at 2100 CE for Alaska and Western Canada & USA regions using the 3-D viscoelastic Earth model. (b) The contribution to the RSL from VLM over the same period. (c) The remaining signal after subtracting (b) from (a), which is the change in SSH.

predicts a sea-level fall of ∼22 cm, the viscoelastic Earth model shows a sea-level rise of ∼5 cm giving a difference of ∼26 cm when compared to the elastic Earth model results.

In RGI region 2, (Figure 2-9, bottom panels), Vancouver, Canada, shows a sea level fall of ∼6 cm when using an elastic Earth model; however, the viscoelastic Earth models shows a fall in sea level of only ∼4 cm. While Victoria, Canada, much like Sitka, USA, shows a sea level fall of ∼4 cm with the elastic Earth model, and sea level rise of ∼1.5 cm with the viscoelastic Earth model.

In Sitka, Vancouver, and Victoria we see that, with the viscoelastic Earth model, over time the RSL transitions from a fall to a rise. This is due to these locations being close to what is called the "hinge line": a location in isostatic response that separates the regions of uplift and subsidence. Over the modelled period the hinge line will migrate towards the main centre of loading over time as the ice retreats. Looking at the results for these three locations we can see the non-monotonic nature of the RSL response is governed by that of the VLM and so the SSH contribution will be of secondary importance. The SSH contribution is primarily that of a sea-level fall as the reduced mass of the GIC exert less of a gravitational pull on the surrounding ocean. This fall in SSH offsets some of the sea-level rise caused by the VLM in these locations. In Vancouver, the transition from VLM uplift to subsidence occurs later and so the net VLM change is relatively small. As a result, the lowering of SSH dominates the RSL signal at this location.

Looking at results for the Southern Andes (Figure 2-10), we see again that the lower viscosity in the mantle results in a more rapid sea-level fall in the areas shaded in red. In this region the subsidence of the peripheral bulge is much more subtle than was seen in Alaska and Western Canada & US. This may be due to a difference in the viscosity of the asthenosphere and upper mantle in the two regional Earth models. In the model for Alaska and Western Canada & USA, the values define a relatively thin low viscosity asthenosphere over a high viscosity upper mantle. As a result, we hypothesise that the displacement of the asthenosphere due to the ice mass causes horizontal channel flow, resulting in a more prominent peripheral bulge. The values

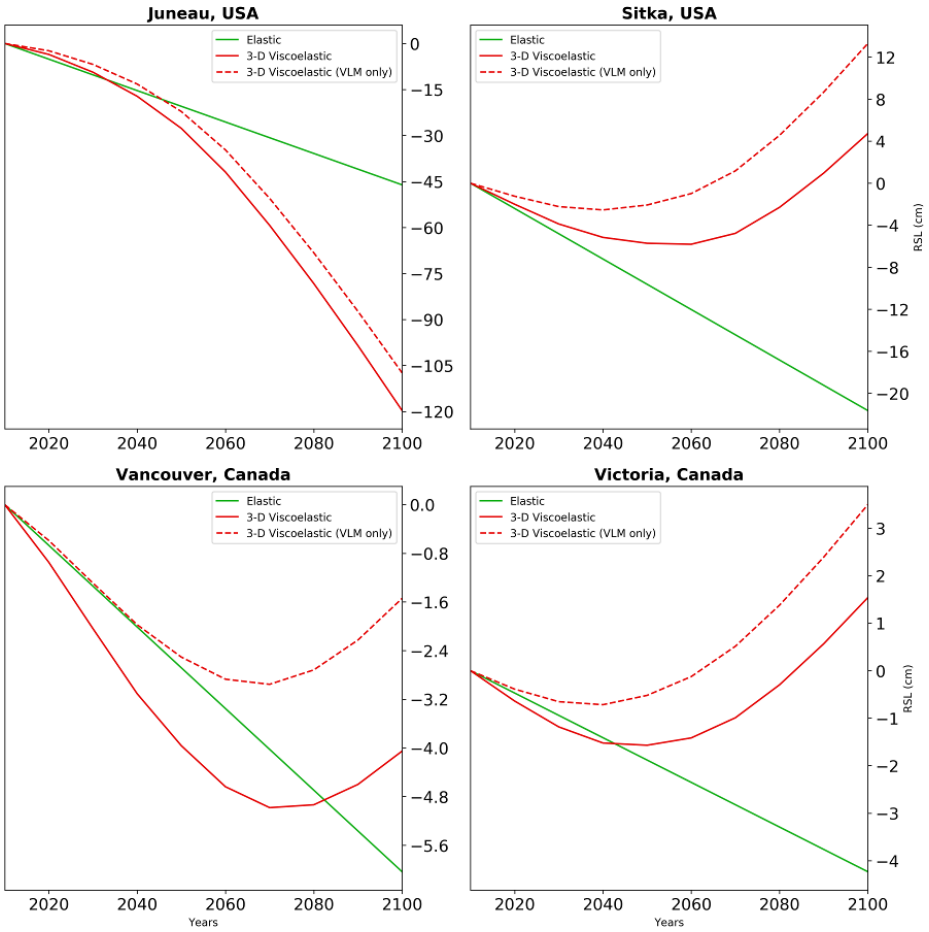

Figure 2-9. Time series plots showing the change in RSL from 2010-2100 CE for the Alaska and Western Canada & USA regions. The green line shows changes using the elastic Earth model, the solid red line shows changes in using the 3-D viscoelastic Earth model, and the dashed red line shows the changes in RSL due to VLM only, using the 3-D viscoelastic Earth model.

used to define the mantle viscosity structure for the Southern Andes on the other hand do not differentiate between the asthenosphere and upper mantle and therefore this region has a low viscosity from the base of the lithosphere to the base of the upper mantle.

To confirm that the difference in RSL is again being dominated by changes in VLM, we isolate the components of the RSL signal in Figure 2-8. Once we remove the VLM (Figure 2-8b) from the total RSL signal (Figure 2-8a) we can confirm that VLM is the dominant signal.

Figure 2-12 shows time series plots for two locations in the Southern Andes region. In the near field we can see that for Puerto Natales, Chile, the elastic Earth model (green line) shows a sea-level fall of $\sim$6.5 cm while the viscoelastic Earth model (solid red line) is showing a sea-level fall of $\sim$11.5 cm. As with Juneau, USA, this is the result of rapid uplift of the solid Earth due to a significantly lower upper mantle viscosity. The VLM (dashed red line) dominates the signal with only $\sim$2 cm of the change in RSL being caused by the SSH component. At Río Grande, Argentina, we see that the elastic Earth model shows a sea-level fall of $\sim$3.2 cm while the viscoelastic Earth model gives a fall of $\sim$1.2 cm. We see a time series similar to the one for Sitka, Vancouver, and Victoria where the viscoelastic results initially start as a sea-level fall before transitioning to a sea-level rise. Again, this is due to the location of this site relative to the hinge line. For the case of Río Grande, the timing of the transition of uplift to subsidence is such that the net contribution of VLM to RSL is zero and so sea-surface fall is the dominant factor.

While this study assumes a Maxwell rheology, there is the possibility that, on these short time scales, a significant transient component of deformation is present. In this case, because the short-term response is generally faster when there is a transient component, the effective viscosity could potentially be lower by 1 to 2 orders of magnitude (Pollitz, 2019) compared to that of steady state creep as simulated by a Maxwell rheology. This further reduction in viscosity would result in a more rapid response of the solid Earth than has been shown in these results.

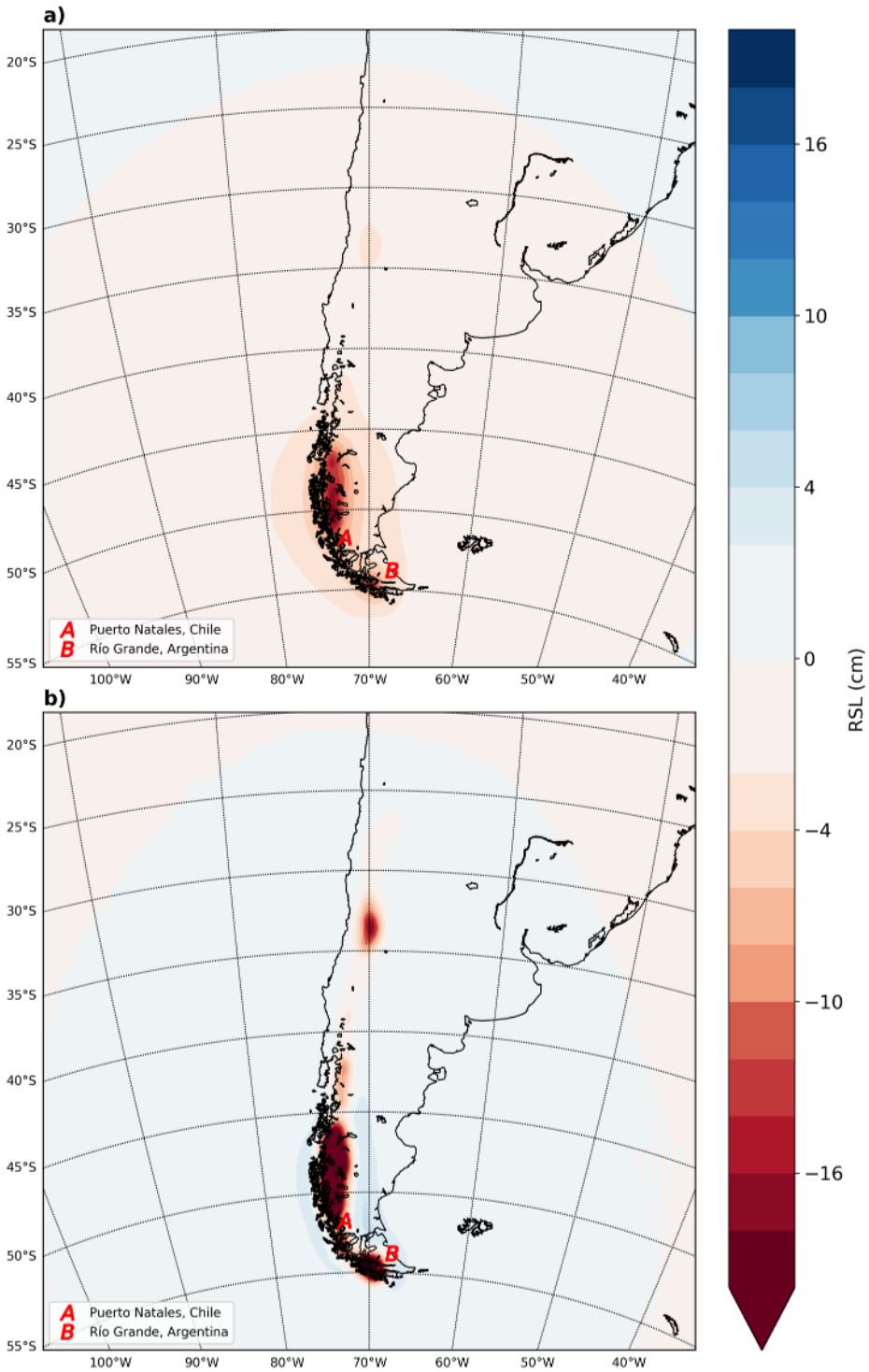

Figure 2-10. (a) The RSL elastic Earth model results for the Southern Andes region at 2100 CE. (b) The difference in RSL between the viscoelastic and elastic Earth models for the same regions and period.

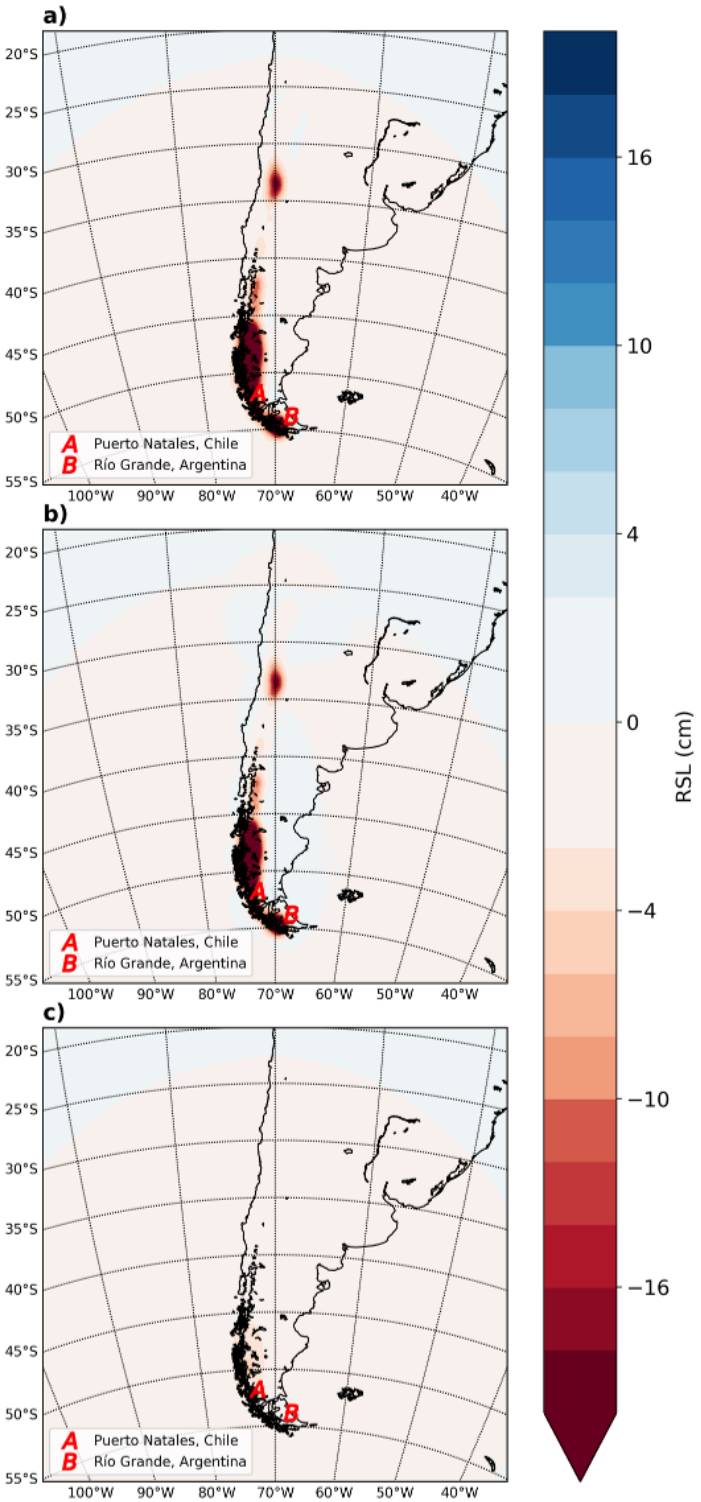

Figure 2-11. (a) The total change in RSL at 2100 CE for the Southern Andes region using the 3-D viscoelastic Earth model. (b) The contribution to the RSL from VLM over the same period. (c) The remaining signal after subtracting (b) from (a), which is the change in SSH.

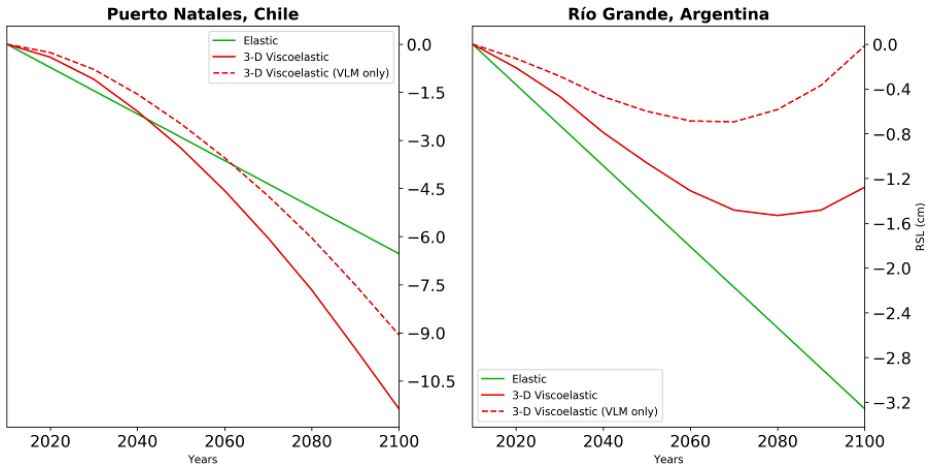

Figure 2-12. Time series plots showing the change in RSL from 2010-2100 CE for the Southern Andes region. The green line shows changes using the elastic Earth model and the red line shows changes in using the 3-D viscoelastic Earth model.

2.4 Concluding remarks

On comparing results from an elastic Earth model with those from a model that includes low viscosity material beneath three of the 19 RGI regions, we conclude that projecting sea level change using an elastic Earth model is sufficient when considering areas in the far-field and is accurate to within ∼2 cm when considering in the intermediate field. However, the elastic Earth model results in large errors when considering locations in the near-field.

Many communities along the northwest coast of Canada and the southern coast of Alaska will need to take into account the viscoelastic response of the mantle when considering sea-level projections. Locations like Sitka, USA, located on a peripheral bulge, are particularly vulnerable due to the elastic Earth model projecting a sea-level fall while the viscoelastic Earth model projects a sea-level rise. This discrepancy could significantly influence the decisions made by policy makers for these locations.

In the Southern Andes region, most of the densely populated locations are on the East coast, in the intermediate-field, and therefore only experience moderate differences based on our elastic and viscoelastic projections. The majority of the near-field is sparsely populated.

When considering the importance of the GIA response in these low viscosity re-

gions, we can see from the time series plots that there can be a strong acceleration in the VLM.

It is important to keep in mind that the sea-level fingerprints presented above are only one component that contributes to sea-level change and so these need to be combined with other factors that will also contribute to regional sea-level change. For example, the sea-level fall resulting from the rapid uplift of the solid Earth could offset some of the sea-level rise from thermal expansion of the ocean reducing the overall impact.

While this work shows that a 3-D viscoelastic earth model is required to determine accurate projections of sea-level fingerprints in near-field locations underlain by low viscosity rock, future work is required to improve the accuracy of the projections. Further work is necessary to more accurately define the radial and lateral boundaries of the low viscosity regions as this will have a direct impact on the projections. Additionally, in regions where subduction is occurring it may be beneficial to explicitly incorporate the geometry of the subducting plate into the model (e.g. Austermann et al., 2013), rather than the simpler 1-D profiles adopted here.

The use of higher resolution regional models would also be able to more accurately define the boundaries of the ice model. While there are indications that Iceland has local viscosity that is several orders of magnitude lower than typical global mean values (Compton et al., 2015), it was not included in this study because the GIC in this region were too small to work with on a global scale model. Therefore, it should also be considered in future work using models that make used of higher resolution (nested) grids. Furthermore, as shown here, our results are sensitive to the location of a given site relative to the ice margin and so use of a nested (higher resolution) grid will enable the ice margins to be more precisely defined.

3

Conclusion

Predicting sea-level rise is one of the great scientific challenges of our time and while the global average change is a useful single value representing a good estimate of sea level change at many coastal locations, there are various regional processes that can produce a strong signal which can result in large departures from the global average value (Church et al., 2013).

Although glaciers and ice caps (GIC) represent less than one percent of the land ice on Earth, their melt water has contributed nearly one third of the observed sea level rise since 1971 and over the next century it is projected to be the second largest contributor to sea level rise (Church et al., 2013). Because of this, understanding RSL changes on a global and local scale, associated with mass loss of GIC, is vital in planning for the impact rising sea level will have on coastal communities.

Projecting local and regional sea level change involves the interaction of numerous

processes driving changes in the vertical movement of either the solid Earth or the ocean surface along any coast. The interactions emerge as complex patterns of sea level change that varies through time as the relative contribution of each process changes. As a result, projecting sea level changes at the local and regional scale requires understanding numerous physical processes that have a wide range of spacial scales and response times.

This thesis looked at the contribution of GIC to future sea-level rise projections and the role that the viscosity of the upper mantle plays in the creation of patterns of RSL change in the form of sea-level fingerprints. Historically, the computation of sea-level fingerprints have not included the viscous component of the Earth's mantle because the non-elastic deformation of the solid Earth over decadal and centennial timescales due to ice loading is only a very small component in most regions. However, recent studies have provided evidence that the glaciated regions of Alaska, Western Canada & USA, and the Southern Andes have a local upper mantle viscosity that is several orders of magnitude lower than typical global mean values and the viscous component of deformation can potentially be significant. Therefore, sea-level fingerprints computed using an elastic Earth model were compared to those computed using a 3-D viscoelastic Earth model for these regions.

When considering locations in the far-field of GIC regions with low mantle viscosity, it was found that the effects are negligible, while for locations in the intermediate-field it was found that the results based on a elastic Earth model are accurate to within $\sim$2 cm. However, when looking at locations in the near-field there may potentially be large errors (several 10s of cm in some coastal areas) when using an elastic Earth model.

In the Alaska and Western Canada & USA regions, four population centres were considered, Juneau and Sitka in the USA and Vancouver and Victoria in Canada. In Juneau it was found that the sea-level fall projected by the viscoelastic Earth model was more than double that of the sea-level fall projected using an elastic Earth model ($\sim$120 cm vs. $\sim$46 cm by 2100 CE). In Sitka and Victoria, the results for the elastic Earth model showed a sea-level fall, but the viscoelastic Earth model results showed a

sea-level rise (a net difference of ∼26 cm and ∼6 cm respectively, by 2100 CE). This is due to the viscoelastic Earth model including the subsidence of the peripheral bulge of the nearby ice mass. In Vancouver a similar trend was seen, and while both Earth models project a sea-level fall, the viscoelastic Earth model shows less of a fall (∼4 cm by 2100 CE) than the elastic model (∼6 cm by 2100 CE). Also, due to its distance from the ice load, the RSL signal for Vancouver is dominated by the change in SSH rather than the change in VLM.

In the Southern Andes region, the cities of Puerto Natales, Chile and Río Grande, Argentina were considered. The results for Puerto Natales are similar to those found in Juneau where the sea-level fall projected by the viscoelastic Earth model is over 50% greater than the sea-level fall projected by the elastic Earth model (∼11 cm vs. ∼7 cm by 2100 CE). In Río Grande the results were similar to those in Vancouver where both models project a sea-level fall, but the fall projected by the elastic model are more than double that of the viscoelastic model (∼3 cm vs. ∼7 cm by 2100 CE) with the RSL signal being dominated by the change in SSH.

While this thesis has shown the importance of using a 3-D viscoelastic Earth model when projecting RSL change for regions with low upper mantle viscosity, future work is necessary to improve the accuracy of these projections. Firstly, since the differences are only large in the near-field, a higher resolution regional grid could be used instead of a global grid to more accurately define the lateral boundaries of smaller GIC. While there is evidence that Iceland also has an upper mantle viscosity that is lower than the global average, it was left out of this study because of this limitation in spatial resolution. Secondly, uncertainties could be explored further by both computing sea-level fingerprints using other RCP scenarios and by considering a range of plausible viscosity models for each region. In relation to this latter point, the low viscosity in all three regions considered here is thought to be related to the presence of a hydrated "mantle wedge" above a subducting plate. This structure could be explicitly included within the Earth model in future studies. Lastly, the inclusion of a transient component of deformation in the Earth model could be explored.

As our climate continues to change our ability to accurately project future sea-

levels becomes increasingly important for both scientists and policy makers. While sea-level fingerprints are just one of several components that contribute to sea-level change, their effect can appear to be counterintuitive. Therefore, it is important to have models that can accurately project how they will impact coastal communities. As this study has shown, the effects of a low viscosity upper mantle could intensify or mitigate other contributing components of sea-level change.

Bibliography

Arendt, A et al. (2015). "Randolph Glacier Inventory–A Dataset of Global Glacier Outlines: Version 5.0". In: *Global Land Ice Measurements from Space, Boulder CO, USA*.

Austermann, Jacqueline et al. (2013). "Barbados-based estimate of ice volume at Last Glacial Maximum affected by subducted plate". In: *Nature Geoscience* 6.7, p. 553.

Botella, Albéric (2015). "Past and Future Sea-Level Changes in French Polynesia". PhD thesis. Université d'Ottawa/University of Ottawa.

Church, J.A. et al. (2013). "Sea Level Change". In: *Climate Change 2013: The Physical Science Basis. Contribution of Working Group I to the Fifth Assessment Report of the Intergovernmental Panel on Climate Change*. Ed. by T.F. Stocker et al. Cambridge, United Kingdom and New York, NY, USA: Cambridge University Press. Chap. 13, pp. 1137–1216.

Clark, James A, William E Farrell, and W Richard Peltier (1978). "Global Changes in Postglacial Sea Level: A Numerical Calculation 1". In: *Quaternary Research* 9.3, pp. 265–287.

Cogley, J Graham et al. (2011). *Glossary of glacier mass balance and related terms, IHP-VII technical documents in hydrology No. 86, IACS Contribution No. 2.*

Collins, M. et al. (2013). "Long-term Climate Change: Projections, Commitments and Irreversibility". In: *Climate Change 2013: The Physical Science Basis. Contribution of Working Group I to the Fifth Assessment Report of the Intergovernmental*

Panel on Climate Change. Ed. by T.F. Stocker et al. Cambridge, United Kingdom and New York, NY, USA: Cambridge University Press. Chap. 12, pp. 1029–1136.

Compton, Kathleen, Richard A Bennett, and Sigrún Hreinsdóttir (2015). "Climate-driven vertical acceleration of Icelandic crust measured by continuous GPS geodesy". In: *Geophysical Research Letters* 42.3, pp. 743–750.

Cuffey, Kurt M and William Stanley Bryce Paterson (2010). *The physics of glaciers*. Academic Press.

Dziewonski, Adam M and Don L Anderson (1981). "Preliminary reference Earth model". In: *Physics of the earth and planetary interiors* 25.4, pp. 297–356.

Farrell, WE and James A Clark (1976). "On postglacial sea level". In: *Geophysical Journal International* 46.3, pp. 647–667.

Gregory, Jonathan M et al. (2013). "Twentieth-century global-mean sea level rise: Is the whole greater than the sum of the parts?" In: *Journal of Climate* 26.13, pp. 4476–4499.

Griggs, Gary (2017). *Coasts in Crisis: A Global Challenge*. Univ of California Press.

Hartmann, D.L. et al. (2013). "Observations: Atmosphere and Surface". In: *Climate Change 2013: The Physical Science Basis. Contribution of Working Group I to the Fifth Assessment Report of the Intergovernmental Panel on Climate Change*. Ed. by T.F. Stocker et al. Cambridge, United Kingdom and New York, NY, USA: Cambridge University Press. Chap. 2, pp. 159–254.

Hay, Carling C et al. (2017). "Sea Level Fingerprints in a Region of Complex Earth Structure: The Case of WAIS". In: *Journal of Climate* 30.6, pp. 1881–1892.

Huss, Matthias and Daniel Farinotti (2012). "Distributed ice thickness and volume of all glaciers around the globe". In: *Journal of Geophysical Research: Earth Surface* 117.F4.

Huss, Matthias and Regine Hock (2015). "A new model for global glacier change and sea-level rise". In: *Frontiers in Earth Science* 3, p. 54.

IPCC (2013). "Annex III: Glossary". In: *Climate Change 2013: The Physical Science Basis. Contribution of Working Group I to the Fifth Assessment Report of the Intergovernmental Panel on Climate Change*. Ed. by T.F. Stocker et al. Cam-

bridge, United Kingdom and New York, NY, USA: Cambridge University Press. Chap. AIII, pp. 1447–1466.

James, Thomas S et al. (2009). "Viscosity of the asthenosphere from glacial isostatic adjustment and subduction dynamics at the northern Cascadia subduction zone, British Columbia, Canada". In: *Journal of Geophysical Research: Solid Earth* 114.B4.

Jin, Shuanggen, TY Zhang, and F Zou (2017). "Glacial density and GIA in Alaska estimated from ICESat, GPS and GRACE measurements". In: *Journal of Geophysical Research: Earth Surface* 122.1, pp. 76–90.

Kendall, Roblyn A, Jerry X Mitrovica, and Glenn A Milne (2005). "On post-glacial sea level–II. Numerical formulation and comparative results on spherically symmetric models". In: *Geophysical Journal International* 161.3, pp. 679–706.

Kopp, Robert E et al. (2016). "Temperature-driven global sea-level variability in the Common Era". In: *Proceedings of the National Academy of Sciences* 113.11, E1434–E1441.

Latychev, Konstantin et al. (2005). "Glacial isostatic adjustment on 3-D Earth models: a finite-volume formulation". In: *Geophysical Journal International* 161.2, pp. 421–444.

Love, Ryan et al. (2016). "The contribution of glacial isostatic adjustment to projections of sea-level change along the Atlantic and Gulf coasts of North America". In: *Earth's Future* 4.10, pp. 440–464.

Masson-Delmotte, V. et al. (2013). "Information from Paleoclimate Archives". In: *Climate Change 2013: The Physical Science Basis. Contribution of Working Group I to the Fifth Assessment Report of the Intergovernmental Panel on Climate Change*. Ed. by T.F. Stocker et al. Cambridge, United Kingdom and New York, NY, USA: Cambridge University Press. Chap. 5, pp. 383–464.

Milne Glenn, A and X Mitrovica Jerry (1998). "Postglacial sea-level change on a rotating Earth". In: *Geophysical Journal International* 133.1, pp. 1–19.

Milne, Glenn A (2014). "Sea Level". In: *Coastal Environments and Global Change*. John Wiley & Sons. Chap. 2, pp. 28–51.

— (2015). “Glacial isostatic adjustment”. In: *Handbook of Sea-Level Research*. John Wiley & Sons. Chap. 28, pp. 421–437.

Mitrovica, Jerry X et al. (2005). “The rotational stability of an ice-age earth”. In: *Geophysical Journal International* 161.2, pp. 491–506.

Mitrovica, JX et al. (2011). “On the robustness of predictions of sea level fingerprints”. In: *Geophysical Journal International* 187.2, pp. 729–742.

Molnia, Bruce F (2005). *Pedersen Glacier*. From the Glacier Photograph Collection. Boulder, Colorado USA: National Snow and Ice Data Center. Digital media.

Nicholls, R. J. et al. (2008). *Ranking Port Cities with High Exposure and Vulnerability to Climate Extremes*.

Pedersen, Louis H (1917). *Pedersen Glacier*. From the Glacier Photograph Collection. Boulder, Colorado USA: National Snow and Ice Data Center. Digital media.

Peltier, WR (2004). “Global glacial isostasy and the surface of the ice-age Earth: the ICE-5G (VM2) model and GRACE”. In: *Annu. Rev. Earth Planet. Sci.* 32, pp. 111–149.

Pollitz, Fred F (2019). “Lithosphere and shallow asthenosphere rheology from observations of post-earthquake relaxation”. In: *Physics of the Earth and Planetary Interiors* 293, p. 106271.

Rhein, M. et al. (2013). “Observations: Ocean”. In: *Climate Change 2013: The Physical Science Basis. Contribution of Working Group I to the Fifth Assessment Report of the Intergovernmental Panel on Climate Change*. Ed. by T.F. Stocker et al. Cambridge, United Kingdom and New York, NY, USA: Cambridge University Press. Chap. 3, pp. 255–316.

Richter, A et al. (2016). “Crustal deformation across the Southern Patagonian Icefield observed by GNSS”. In: *Earth and Planetary Science Letters* 452, pp. 206–215.

Roemmich, Dean and John Gilson (2009). “The 2004–2008 mean and annual cycle of temperature, salinity, and steric height in the global ocean from the Argo Program”. In: *Progress in oceanography* 82.2, pp. 81–100.

Ruddiman, William F (2001). *Earth’s Climate: past and future*. Macmillan.

Slangen, ABA et al. (2012). "Towards regional projections of twenty-first century sea-level change based on IPCC SRES scenarios". In: *Climate dynamics* 38.5-6, pp. 1191–1209.

Slangen, ABA et al. (2014). "Projecting twenty-first century regional sea-level changes". In: *Climatic Change* 124.1-2, pp. 317–332.

Whitehouse, Pippa L (2018). "Glacial isostatic adjustment modelling: historical perspectives, recent advances, and future directions". In: *Earth surface dynamics* 6.2, pp. 401–429.

Whitehouse, Pippa L et al. (2019). "Solid Earth change and the evolution of the Antarctic Ice Sheet". In: *Nature communications* 10.1, pp. 1–14.

Yousefi, Maryam et al. (2018). "Glacial isostatic adjustment along the Pacific coast of central North America". In: *Quaternary Science Reviews* 193, pp. 288–311.

Zemp, Michael et al. (2015). "Historically unprecedented global glacier decline in the early 21st century". In: *Journal of Glaciology* 61.228, pp. 745–762.